AGU PUBLICATIONS

Water Resources Research

RESEARCH ARTICLE
10.1002/2015WR017200

Companion to *Clark et al.* [2015], doi:10.1002/2015WR017198.

Key Points:
- Flexible model implementation enables evaluation of key modeling decisions
- Case studies illustrate capabilities to identify preferable modeling approaches
- Accelerates improvements in model fidelity & uncertainty characterization

Correspondence to:
M. P. Clark,
mclark@ucar.edu

Citation:
Clark, M. P. et al. (2015), A unified approach for process-based hydrologic modeling: 2. Model implementation and case studies, *Water Resour. Res.*, *51*, 2515–2542, doi:10.1002/2015WR017200.

Received 6 MAR 2015
Accepted 10 MAR 2015
Accepted article online 16 MAR 2015
Published online 20 APR 2015

A unified approach for process-based hydrologic modeling: 2. Model implementation and case studies

Martyn P. Clark[1], Bart Nijssen[2], Jessica D. Lundquist[2], Dmitri Kavetski[3], David E. Rupp[4], Ross A. Woods[5], Jim E. Freer[6], Ethan D. Gutmann[1], Andrew W. Wood[1], David J. Gochis[1], Roy M. Rasmussen[1], David G. Tarboton[7], Vinod Mahat[8], Gerald N. Flerchinger[9], and Danny G. Marks[9]

[1]Hydrometeorological Applications Program, Research Applications Laboratory, National Center for Atmospheric Research, Boulder, Colorado, USA, [2]Department of Civil and Environmental Engineering, University of Washington, Seattle, Washington, USA, [3]School of Civil, Environmental and Mining Engineering, University of Adelaide, Adelaide, South Australia, Australia, [4]Oregon Climate Change Research Institute, College of Earth, Ocean, and Atmospheric Sciences, Oregon State University, Corvallis, Oregon, USA, [5]Faculty of Engineering, University of Bristol, Bristol, UK, [6]School of Geographical Sciences, University of Bristol, Bristol, UK, [7]Department of Civil and Environmental Engineering, Utah Water Research Laboratory, Utah State University, Logan, Utah, USA, [8]Department of Civil and Environmental Engineering, Colorado State University, Fort Collins, Colorado, USA, [9]Northwest Watershed Research Center, USDA-Agricultural Research Service, Boise, Idaho, USA

Abstract This work advances a unified approach to process-based hydrologic modeling, which we term the "Structure for Unifying Multiple Modeling Alternatives (SUMMA)." The modeling framework, introduced in the companion paper, uses a general set of conservation equations with flexibility in the choice of process parameterizations (closure relationships) and spatial architecture. This second paper specifies the model equations and their spatial approximations, describes the hydrologic and biophysical process parameterizations currently supported within the framework, and illustrates how the framework can be used in conjunction with multivariate observations to identify model improvements and future research and data needs. The case studies illustrate the use of SUMMA to select among competing modeling approaches based on both observed data and theoretical considerations. Specific examples of preferable modeling approaches include the use of physiological methods to estimate stomatal resistance, careful specification of the shape of the within-canopy and below-canopy wind profile, explicitly accounting for dust concentrations within the snowpack, and explicitly representing distributed lateral flow processes. Results also demonstrate that changes in parameter values can make as much or more difference to the model predictions than changes in the process representation. This emphasizes that improvements in model fidelity require a sagacious choice of both process parameterizations and model parameters. In conclusion, we envisage that SUMMA can facilitate ongoing model development efforts, the diagnosis and correction of model structural errors, and improved characterization of model uncertainty.

1. Introduction

The development of process-based hydrologic models is a complex interdisciplinary pursuit. Key challenges include selecting appropriate modeling approaches to simulate land-atmosphere energy fluxes (including transpiration), canopy interception, snow accumulation and ablation, partially frozen soil, overland flow, and representing the highly heterogeneous storage and transmission of liquid water through the catchment. These challenges are exacerbated by issues of scale [*Mahrt*, 1987; *Reggiani et al.*, 1998; *Zehe et al.*, 2006; *Essery et al.*, 2008] and difficulties in estimating spatially distributed model parameters and meteorological model inputs [*Freeze and Harlan*, 1969; *Maxwell and Kollet*, 2008; *Samaniego et al.*, 2010; *Montanari and Koutsoyiannis*, 2012].

Given this complex set of challenges, the development of hydrologic models requires a controlled and systematic approach [*Clark et al.*, 2011]. This can be accomplished using modeling methodologies designed to evaluate multiple alternative process representations, which are treated as multiple working hypotheses. Such methodologies have previously been explored in appreciable depth in the field of "conceptual" hydrological modeling [*Moore and Clarke*, 1981; *Clark et al.*, 2008; *Fenicia et al.*, 2011]. In a recent application of these ideas to "physically explicit" models, *Niu et al.* [2011] compared different model options for

representing turbulent heat transfer, soil moisture stress and snow processes, and were able to attribute differences in overall model performance to specific modeling decisions. Similarly, *Essery et al*. [2013] compared different model options for snow compaction, time evolution of snow surface albedo, and storage/transmission of liquid water through the snowpack, and were able to identify specific modeling options that resulted in poor model performance. These expanded applications of the method of multiple working hypotheses to process-based models provide useful insights for model development.

This two-part paper builds on the existing literature of modeling methodologies that integrate multiple modeling alternatives [*Moore and Clarke*, 1981; *Leavesley et al*., 2002; *Pomeroy et al*., 2007; *Clark et al*., 2008; *Best et al*., 2011; *Fenicia et al*., 2011; *Niu et al*., 2011; *Essery et al*., 2013] by introducing and applying a new modeling framework, the Structure for Unifying Multiple Modeling Alternatives (SUMMA), for the systematic analysis of competing modeling options [*Clark et al*., 2015b]. SUMMA advances the existing modeling frameworks by (i) supporting different model representations of spatial variability and hydrologic connectivity, enabling analysis of the effects of the choice of the spatial discretization approach and the representation of lateral flow processes on basin-wide runoff and evapotranspiration fluxes; (ii) supporting a broad range of biophysical and hydrologic modeling options, enabling analysis of both the impacts of model simplification and the impacts of the choice of modeling approaches for individual physical processes; (iii) supporting analysis of a broad range of model parameter values, providing flexibility to evaluate the interplay between the choice of model parameters and the choice of process parameterizations; and (iv) separating modeling decisions on process representation from their numerical implementation, providing capabilities to experiment with different numerical solvers.

The development of SUMMA in the first paper [*Clark et al*., 2015b] focuses on the spatial organization and model simplifications, on how different representations of multiple physical processes can be combined within a single modeling framework, and on our broader vision for using SUMMA in environmental modeling. Our intent for the first paper is to advance a general methodology for the application of the method of multiple working hypotheses in hydrologic and land-surface models (i.e., define a general master modeling template from which existing models can be constructed and new models derived).

This second paper builds on the motivation for SUMMA in the first paper and introduces the initial implementation of SUMMA as a modeling system. The goals of this second paper are (i) present the model equations and their spatial approximations; (ii) describe multiple options for the dominant biophysical and hydrologic processes (i.e., the flux terms in the conservation equations); and (iii) illustrate how SUMMA can be used to identify preferable process parameterizations and to pinpoint model weaknesses. The processes considered in this paper include radiation transfer through the vegetation canopy, within-canopy and below-canopy turbulence, canopy interception, canopy transpiration, snow accumulation and ablation, and runoff generation. In all cases, we examine the choice of equations used to parameterize specific processes, along with the choice of parameter values used in the model equations.

The remainder of the paper is organized as follows. Sections 2 and 3 specify the conservation equations, along with the multiple parameterizations for the different thermodynamic and hydrologic fluxes. Section 4 defines the spatial and temporal approximations used in the numerical solution. Based on this development, Section 5 presents initial applications of SUMMA for several research catchments throughout the western USA. Finally, section 6 summarizes the initial findings and discusses major outstanding research questions.

2. Conservation Equations

SUMMA's model domain extends from the atmosphere above the vegetation canopy to the river channel and includes the dominant biophysical and hydrologic processes for many regions of the world [see *Clark et al*., 2015b, Figure 1]. We simulate thermodynamics, i.e., the storage and flux of energy, and hydrology, i.e., the storage and transmission of water (in all of its phases). For thermodynamics, we define conservation equations that describe the heat balance of the vegetation canopy, the canopy air space, snow, and soil, as affected by the radiative fluxes through the vegetation canopy, within-canopy and below-canopy turbulent heat transfer, and energy fluxes throughout the snow and soil. For hydrology, we define conservation equations that describe the water balance of the vegetation, snow, and soil, as affected by the fluxes of interception and unloading (or drip) of snow (or rain) from the vegetation canopy, snowfall, snow melt, and

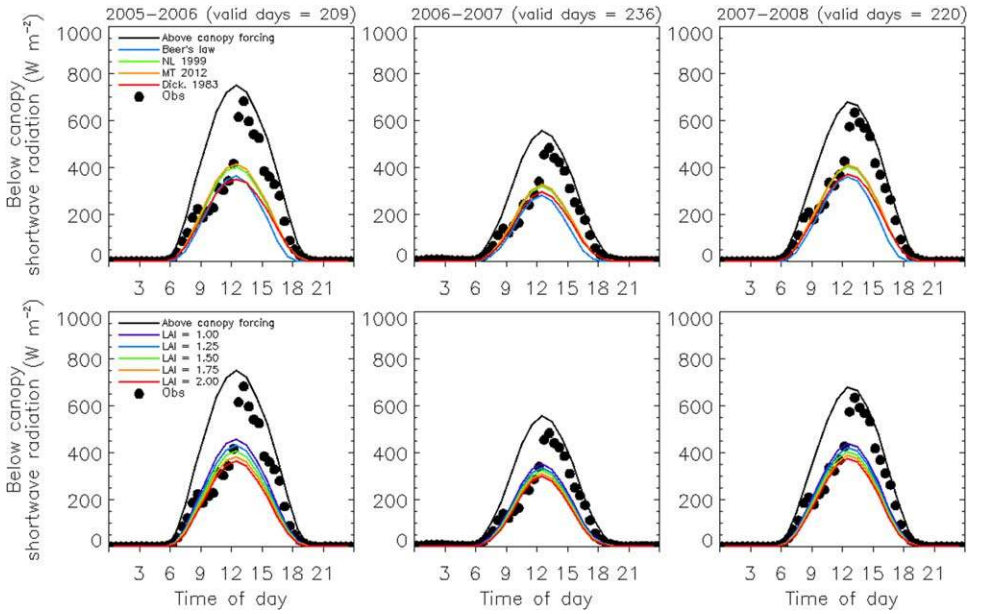

Figure 1. Impact of the choice of canopy shortwave radiation parameterizations and the choice of model parameter values on simulations of below canopy shortwave radiation for three representative water years at the aspen site in the Reynolds Mountain East basin, showing (top row) impact of canopy shortwave radiation parameterizations; and (bottom row) impact of the Leaf Area Index, as used in the parameterization described by *Mahat and Tarboton* [2012]. Note that the below-canopy observations are close to the above-canopy forcing in the early afternoon period, indicating a gap in the canopy that is not represented with diurnally constant model parameters. The observations (circles) are described in *Flerchinger et al*. [2012].

sublimation, vertical and lateral transmission of liquid water through snow and soil, the storage and transmission of water in the shallow subterranean aquifer, and transpiration, canopy evaporation, and ground evaporation.

In presenting the model equations, we use the following rules to maintain a consistent notation. All vertical fluxes are defined as positive downward. Turbulent energy fluxes from the canopy to the canopy air space are defined as positive toward the canopy, and lateral fluxes of liquid water within the soil profile and subterranean aquifer are defined as positive downslope. Superscripts are used to define the model subdomain (the superscripts *cas*, *veg*, *snow*, and *soil* denote the canopy air space, the vegetation canopy, snow, and soil, respectively, and the superscript *ss* denotes the snow and soil subdomain). Subscripts are used to define the additional characteristics as needed, such as the type of constituent within a model subdomain (the subscripts *liq*, *ice*, *veg*, *soil*, and *air* denote the constituents of liquid water, ice, vegetation, soil, and air). The variable z (m) defines the vertical coordinate (positive downward) and h (m) defines the height above the soil surface (positive upwards), where $z = 0$ and $h = 0$ define the height of the soil surface. The abbreviations LHS and RHS are used to refer to the left-hand side and right-hand side of the model equations.

Control volumes within the model are represented as a mixture of constituents [e.g., *Jordan*, 1991]

$$\sum_k \theta_k = 1 \tag{1}$$

where θ_k (-) is the volumetric fraction of the k-th constituent, and the subscript ($k = liq$, ice, veg, $soil$, air) denotes the constituents of liquid water, ice, vegetation, soil, and air.

The bulk density γ_k (kg m^{-3}) of constituent k (i.e., the mass of constituent k per unit volume) is related to the intrinsic density, ρ_k (kg m^{-3}), as

$$\gamma_k = \rho_k \theta_k \tag{2}$$

where ρ_{ice} and ρ_{liq} are constant ($\rho_{ice} = 917$ and $\rho_{liq} = 1000$ kg m^{-3}, respectively), ρ_{air} depends on the meteorological conditions, and ρ_{soil} depends on the soil properties.

The volumetric specific heat capacity, C_p (J m^{-3} K^{-1}), can then be defined as

$$C_p = \sum_k \gamma_k c_k \tag{3}$$

where c_k (J kg^{-1} K^{-1}) is the specific heat of the k-th constituent.

2.1. Thermodynamics

The thermodynamic state of the system depends on the radiative energy fluxes through the vegetation canopy, turbulent heat fluxes within the canopy, and diffusion of heat throughout the snow-soil system. We only consider energy fluxes in the vertical dimension (lateral energy fluxes are assumed to be zero).

2.1.1. Vegetation Canopy

The conservation equation describing the change in stored energy for the vegetation canopy is

$$C_p^{veg}\frac{\partial T^{veg}}{\partial t} - \rho_{ice}L_{fus}\left[\frac{\partial \theta_{ice}^{veg}}{\partial t}\right]_{mf} = -\frac{\partial(Q_{swd}+Q_{lwd}+Q_{swu}+Q_{lwu}+Q_p)}{\partial z} + H_{sen}^{veg} + H_{lat}^{veg} \tag{4}$$

The first term on the LHS of equation (4) defines the rate of change of canopy temperature T^{veg} (K), and the second term describes the rate of change of canopy volumetric ice content θ_{ice}^{veg} (-) associated with melt-freeze processes (as defined by the subscript *mf*), where an increase in θ_{ice}^{veg} is freezing and a decrease is melting. In equation (4), L_{fus} (J kg^{-1}) is a physical constant defining the latent heat of fusion and T^{veg} is the bulk temperature of all constituents in the vegetation control volume (vegetation, liquid water, and ice, excluding air).

The RHS of equation (4) defines the energy fluxes, where Q_{swd} and Q_{lwd} (W m^{-2}) are the downwelling shortwave and longwave radiation fluxes, Q_{swu} and Q_{lwu} (W m^{-2}) are the upwelling shortwave and longwave radiation fluxes, Q_p (W m^{-2}) is heat advected with precipitation, and H_{sen}^{veg} (W m^{-3}) and H_{lat}^{veg} (W m^{-3}) are the volumetric sensible and latent heat fluxes, respectively, from the vegetation elements to the air space within the canopy (H_{sen}^{veg} and H_{lat}^{veg} are defined as positive toward the vegetation elements).

The total volumetric latent heat flux associated with evapotranspiration is defined as

$$H_{lat}^{veg} = L_{sub}E_{sub}^{veg} + L_{vap}\left(E_{evap}^{veg} + E_{trans}^{veg}\right) \tag{5}$$

where E_{sub}^{veg}, E_{evap}^{veg}, and E_{trans}^{veg} (kg m^{-3} s^{-1}) are the volumetric rates of canopy sublimation, canopy evaporation and canopy transpiration, and L_{sub} and L_{vap} (J kg^{-1}) define the latent heat of sublimation and vaporization.

2.1.2. The Canopy Air Space

The temperature and the vapor pressure of the canopy air space are influenced by the volumetric sensible and latent heat fluxes from the vegetation elements to the air space within the canopy (as defined in equations (4) and (5)), and by the gradients in the vertical fluxes of sensible and latent heat within the canopy air space, Q_h^{cas} and Q_e^{cas}. The conservation equations can be written as [*Vidale and Stockli*, 2005]

$$C_p^{cas}\frac{\partial T^{cas}}{\partial t} = -\frac{\partial Q_h^{cas}}{\partial z} - H_{sen}^{veg} \tag{6}$$

$$C_w^{cas}\frac{\partial e^{cas}}{\partial t} = -\frac{\partial Q_l^{cas}}{\partial z} - H_{lat}^{veg} \tag{7}$$

where C_p^{cas} (J m^{-3} K^{-1}) is the volumetric storage capacity for heat, C_w^{cas} (J m^{-3} Pa^{-1}) is the volumetric storage capacity for moisture, and e^{cas} (Pa) is the vapor pressure in the canopy air space. Note that the only constituent in the canopy air space is air, so $C_p^{cas} = \rho_{air}c_{air}$.

The boundary conditions for equations (6) and (7) can be given as

$$Q_h^{cas} = \begin{cases} Q_h^{total}; & z = -h_{top}^{veg} \\ Q_h^{sfc}; & z = -h_{bot}^{veg} \end{cases} \tag{8}$$

$$Q_l^{cas} = \begin{cases} Q_l^{total}; & z = -h_{top}^{veg} \\ Q_l^{sfc}; & z = -h_{bot}^{veg} \end{cases} \quad (9)$$

where Q_h^{sfc} and Q_l^{sfc} (W m^{-2}) are the sensible and latent heat fluxes from the ground surface to the bottom of the vegetation canopy, and Q_h^{total} and Q_l^{total} (W m^{-2}) are the sensible and latent heat fluxes from the top of the vegetation canopy to the height of the model forcing.

2.1.3. Snow and Soil

The conservation equation describing the change in stored energy for snow and soil is

$$C_p^{ss} = \frac{\partial T^{ss}}{\partial t} - \rho_{ice} L_{fus} \left[\frac{\partial \theta_{ice}^{ss}}{\partial t} \right]_{mf} = -\frac{\partial F}{\partial z} \quad (10)$$

where T^{ss} denotes the temperature (K) and the superscript *ss* refers to the snow-soil domain. Similar to equation (4) for the vegetation canopy, the first and second terms on the LHS of equation (10) define the temperature change and phase change respectively, and all other terms as defined previously.

The vertical energy flux, F (W m^{-2}), is

$$F = \begin{cases} Q_{swnet}^{sfc} + Q_{lwnet}^{sfc} + Q_h^{sfc} + Q_l^{sfc} + Q_p & z = -h_{sfc} \\ -\lambda \dfrac{\partial T^{ss}}{\partial z} & z > -h_{sfc} \end{cases} \quad (11)$$

where Q_{swnet}^{sfc} and Q_{lwnet}^{sfc} (W m^{-2}) are the net shortwave and net longwave radiation fluxes, Q_h^{sfc} and Q_l^{sfc} (W m^{-2}) are the sensible and latent heat at the height of the surface-atmosphere interface ($z = -h_{sfc}$), Q_p (W m^{-2}) is heat advected with precipitation, and λ (W m^{-1} K^{-1}) is the thermal conductivity within the snow-soil medium, which depends on the mixture of constituents at depth z. In equation (11), h_{sfc} is the height of the snow-atmosphere interface (note z is positive downwards, so h_{sfc} is negative when snow is present and zero otherwise).

The net shortwave radiation flux Q_{swnet}^{sfc} requires an additional equation for snow albedo [*Clark et al.*, 2015a]. Note that equation (11) neglects the penetration of solar radiation into the snowpack.

2.2. Hydrology

2.2.1. Canopy Hydrology

The conservation equation for canopy hydrology is

$$\frac{\partial \Theta_m^{veg}}{\partial t} = -\frac{\partial q_{liq}^{veg}}{\partial z} - \frac{\partial q_{ice}^{veg}}{\partial z} + \frac{E_{evap}^{veg} + E_{sub}^{veg}}{\rho_{liq}} \quad (12)$$

where Θ_m^{veg} is the total equivalent liquid water content, i.e., $\Theta_m^{veg} = \theta_{liq}^{veg} + \rho_{ice}\theta_{ice}^{veg}/\rho_{liq}$, E_{evap}^{veg} and E_{sub}^{veg} (kg m^{-3} s^{-1}) are the volumetric evaporation and sublimation fluxes, and q_{liq}^{veg} and q_{ice}^{veg} (m s^{-1}) are the vertical fluxes of liquid water (thoughfall and canopy drainage) and ice (throughfall and unloading of snow from the canopy). The upper boundary condition for equation (12) is rainfall and snowfall at the top of the canopy.

2.2.2. Snow Hydrology

The conservation equation for the time evolution for liquid water in the snow is

$$\frac{\partial \Theta_m^{snow}}{\partial t} = -\frac{\partial q_{liq,z}^{snow}}{\partial z} - \frac{\partial q_{ice}^{veg}}{\partial z} + \frac{E_{evap}^{snow} + E_{sub}^{snow}}{\rho_{liq}} \quad (13)$$

where, analogously to equation (12), $\Theta_m^{snow} = \theta_{liq}^{snow} + \rho_{ice}\theta_{ice}^{snow}/\rho_{liq}$. On the RHS of equation (13), E_{evap}^{snow} and E_{sub}^{snow} (kg m^3 s^{-1}) are the losses due to evaporation of liquid water within the snowpack and sublimation of ice from the snowpack, and $q_{liq,z}^{snow}$ (m s^{-1}) is the vertical flux of liquid water. The term q_{ice}^{snow} (m s^{-1}) represents the vertical flux of water in solid form,

$$q_{ice}^{snow} = \begin{cases} q_{tf,snow}^{snow} + q_{unload}^{snow} & z = -h_{sfc} \\ 0 & z > -h_{sfc} \end{cases} \quad (14)$$

where $q_{tf,snow}^{snow}$ and q_{unload}^{snow} (m s^{-1}) define the throughfall and unloading fluxes (throughfall is equal to

snowfall over bare ground and at times when the canopy is completely covered with snow). Note that in equation (14) the solid precipitation flux occurs only at the top of the snowpack ($z = -h_{sfc}$).

An additional equation is needed to describe the compaction of the snowpack. This is described in discretized form in section 4.1.4

2.2.3. Soil Hydrology

The conservation equation for soil hydrology is

$$\frac{\partial \Theta_m^{soil}}{\partial t} = \frac{\partial q_{liq,x}^{soil}}{\partial x} + \frac{\partial q_{liq,y}^{soil}}{\partial y} - \frac{\partial q_{liq,z}^{soil}}{\partial z} + \frac{E_{evap}^{soil} + E_{trans}^{soil}}{\rho_{liq}} \tag{15}$$

In contrast to equations (12) and (13) where $\rho_{ice} < \rho_{liq}$, in equation (15) we assume that $\rho_{ice} = \rho_{liq}$, meaning that there is no volume expansion during freezing [*Dal'Amico et al*., 2011], and hence $\Theta_m^{soil} = \theta_{liq}^{soil} + \theta_{ice}^{soil}$.

On the RHS of equation (15), the terms $q_{liq,x}^{soil}$, $q_{liq,y}^{soil}$, and $q_{liq,z}^{soil}$ (m s^{-1}) define the liquid fluxes in the *x*, *y*, and *z* directions, and the terms E_{evap}^{soil} and E_{trans}^{soil} (kg m^{-3} s^{-1}) define the losses due to soil evaporation and transpiration, respectively.

To accommodate both unsaturated and saturated flow through soils, the fluxes on the RHS of equation (15) must be formulated as a function of liquid water matric potential, ψ (m). This requires additional functions to relate the fluxes to the liquid water matric potential and to relate total water matric potential to total water content.

For example, the vertical fluxes of liquid water can be parameterized as a Darcy flux, with infiltration into the soil as the upper boundary condition

$$q_{liq,z}^{soil} = \begin{cases} q_{rain} - q_{ix} - q_{sx} & z = 0 \\ -K^{soil} \dfrac{\partial \psi}{\partial z} + K^{soil} & z > 0 \end{cases} \tag{16}$$

where the depth $z = 0$ defines the position of the soil surface. In equation (16) q_{rain}, q_{ix}, and q_{sx} (m s^{-1}) define rainfall, infiltration-excess runoff and saturation-excess runoff, respectively. Within the soil profile, the two terms of the Darcy flux are the capillary and gravity fluxes, ψ (m) is the liquid water matric potential, and $K^{soil} = f(\psi)$ (m s^{-1}) is the unsaturated hydraulic conductivity of soil, which varies with the liquid water matric potential.

Water retention can be given as

$$\Theta_m^{soil}(\psi_0) = S_*(\psi_0) \tag{17}$$

where $S^*(\cdot)$ is the water retention curve, e.g., the *Van Genuchten* [1980] function, and ψ_0 (m) is the total water matric potential (note that for unfrozen conditions $\Theta_m^{soil} = \theta_{liq}^{soil}$ and $\psi_0 = \psi$).

Liquid water flow in partially frozen soils is driven by strong capillary pressure gradients that develop as ice forms in the larger pore spaces. In this work, we follow the approach adopted by *Zhao et al*. [1997], in which (i) the generalized Clapeyron equation is combined with the water retention curve to separate the total water content Θ_m into the volumetric fractions of liquid water θ_{liq} and ice θ_{ice} (see section 2.3.1 and *Clark et al*. [2015a]); and (ii) ice is treated as part of the solid matrix in order to calculate the liquid water matric potential ψ. Including ice as part of the solid matrix prevents freezing-induced suction under saturated conditions [see also *Noh et al*., 2011; *Painter and Karra*, 2014].

Assuming that ice forms part of the solid matrix, the effective saturation of soils, S_e (-) is given as

$$S_e(\psi_0, T) = \frac{\theta_{liq} - \theta_{res}}{\theta_{sat} - \theta_{ice} - \theta_{res}} \tag{18}$$

where θ_{liq} and θ_{ice} can be computed from ψ_0 and T [*Clark et al*., 2015a], and θ_{sat} and θ_{res} (-) define the porosity and residual volumetric liquid water content. Based on the "freezing equals drying" hypothesis (i.e., the same constitutive functions can be used to relate θ_{liq} to ψ under freezing and drying conditions [*Spaans*

and Baker, 1996]), the liquid water matric potential ψ can then be defined using a constitutive function for the water retention curve, e.g., the *Van Genuchten* [1980] function,

$$\psi(\psi_0, T) = \alpha_{vg}^{-1}\left(S_e^{-1/m_{vg}} - 1\right)^{1/n_{vg}} \tag{19}$$

where α_{vg} (m^{-1}) is the capillary length scale, and the parameters m_{vg} (-) and n_{vg} (-) are parameters related to the pore-size distribution ($m_{vg} = 1 - 1/n_{vg}$).

As noted in the first paper, our overall intent is to provide flexibility in both the choice of flux parameterizations and other closure relations. In the current implementation, we use the mixed form of Richards' equation – i.e., equation (16) combined with equation (15) – to simulate the vertical re-distribution of liquid water within the soil profile. Note that equation (15) can be used to simulate water flow in multiple domains. For example, different state variables and flux parameterizations can be used to simulate the storage and transmission of liquid water in micropores and macropores [e.g., *Simunek et al*., 2003]. Implementing these methods requires the specification of additional parameterizations to describe fluxes of water between the macropore and micropore domains.

2.2.4. Storage and Transmission of Liquid Water in the Subterranean Aquifer

The conservation equation for the subterranean aquifer is

$$\frac{dS^{aq}}{dt} = q_{drain}^{aq} + q_{trans}^{aq} - q_{base}^{aq} \tag{20}$$

where S^{aq} (m) is the water storage in the aquifer, q_{drain}^{aq} (m s^{-1}) is the drainage from the bottom of the soil profile, q_{trans}^{aq} (m s^{-1}) is the transpiration loss from the aquifer (recall that fluxes are defined as positive downward), and q_{base}^{aq} (m s^{-1}) is baseflow from the aquifer to the stream.

2.3. Phase Change

2.3.1. Melt-Freeze

All fluxes on the RHS of equations (4), (6), and (10) are expressed as functions of temperature in the relevant parts of the model domain. However, the LHS of equations (4) and (10) include two state variables (the temperature T and the volumetric ice content θ_{ice}). To close the equations, an additional function is needed to relate T to θ_{ice}. In this paper, we use the differentiable functions

$$\theta_{liq}^{veg} = f(T, \Theta_m) \tag{21}$$

$$\theta_{liq}^{snow} = f(T, \Theta_m) \tag{22}$$

$$\theta_{liq}^{soil} = f(T, \psi_0) \tag{23}$$

where Θ_m (-) is the total equivalent liquid water content, i.e., $\Theta_m = \theta_{liq} + \rho_{ice}\theta_{ice}/\rho_{liq}$, and ψ_0 (m) is the matric potential corresponding to the total water content (liquid and ice).

Equations (21) through (23) allow for a fraction of liquid water at subfreezing temperatures (i.e., supercooled liquid water). While soils can contain a considerable fraction of supercooled liquid water [*Fuchs et al*., 1978; *Spaans and Baker*, 1996], the supercooled liquid water in snow (and vegetation) is negligible, so that equations (21) and (22) should approximate a step function at the freezing point [*Jordan*, 1991]. The volume fraction in each phase (θ_{xx}, $xx = liq$, ice, air), along with the liquid water matric potential in soils ψ, are all diagnostic variables that can be calculated from the state variables Θ_m and T (for vegetation and snow) and ψ_0 and T (for soils).

Note that θ_{liq} and θ_{ice} are interchangeable, as reductions in θ_{ice} are accompanied by corresponding increases in θ_{liq}, i.e., $\rho_{liq}L_f\partial\theta_{liq}/\partial t = -\rho_{ice}L_f\partial\theta_{ice}/\partial t$. In our implementation, we make the choice to express equations (21) through (23) in terms of θ_{liq} rather than θ_{ice}. This choice is made because many frozen soil models use the same soil moisture characteristics functions for freezing and thawing as for wetting and drying, where a linear relationship between T and matric head ψ is incorporated within the nonlinear soil moisture characteristics function relating θ_{liq} and ψ [*Spaans and Baker*, 1996; *Cox et al*., 1999; *Niu and Yang*, 2006; *Dall'Amico et al*., 2011]. The relationships between θ_{liq} and T for vegetation and snow and the relationships between θ_{liq} and T for soil are described in *Clark et al*. [2015a].

2.3.2. Evaporation and Sublimation

Phase changes from liquid water to vapor (evaporation/condensation) and ice to vapor (sublimation/frost) are included in the latent heat flux terms in the thermodynamics calculations, and are coupled with the hydrology calculations as part of the Newton-Raphson iterations (see section 4.2.2).

2.4. Snow Albedo

A general state equation for snow albedo is used here to represent existing models that use semi-empirical albedo parameterizations:

$$\frac{d\alpha_d^{snow}}{dt} = \frac{\rho_{liq} q_{sf}}{S_{ref}} \left(\alpha_{\text{max,d}}^{snow} - \alpha_{\text{min,d}}^{snow} \right) - \kappa_\alpha \left(\alpha_d^{snow} - \alpha_{\text{min,d}}^{snow} \right) \tag{24}$$

where α_d^{snow} (-) is the albedo for diffuse radiation, $\alpha_{\text{max,d}}^{snow}$ and $\alpha_{\text{min,d}}^{snow}$ (-) are the maximum and minimum snow albedo, q_{sf} (m s^{-1}) is the rate of snowfall, S_{ref} (kg m^{-2}) is the mass required for albedo refreshment and κ_α (s^{-1}) is the albedo decay rate The first term on the right represents albedo refreshment (increase in albedo associated with new snow) and the second term on the right represents albedo decay. In equation (24) α_d^{snow} is the model state variable, and the direct-beam albedo is a diagnostic variable typically computed by increasing the diffuse albedo at low solar zenith angles [e.g., *Yang et al*., 1997]. During snowfall events, albedo is constrained to be less than or equal to $\alpha_{\text{max,d}}^{snow}$.

Equation (24) subsumes two fundamental processes that define surface albedo: (1) temporal evolution of the size of the snow grains [*Wiscombe and Warren*, 1980; *Jordan*, 1991; *Tribbeck et al*., 2006] and (2) deposition, burial, and re-emergence of atmospheric particles (dust, soot, etc.) and leaf litter [*Warren and Wiscombe*, 1980; *Melloh et al*., 2001; *Painter et al*., 2007, 2012]. Both of these processes are included in the temporal decay rate κ_α.

3. Process Parameterizations

The model options considered in this initial application of SUMMA are drawn from a number of existing hydrologic and land-surface models, including the Variable Infiltration Capacity (VIC) model [e.g., *Liang et al*., 1994; *Andreadis et al*., 2009], the Community Land Model [*Oleson et al*., 2010; *Lawrence et al*., 2011], the Noah Multiparameterization (Noah-MP) model [*Niu et al*., 2011; *Yang et al*., 2011], the Simultaneous Heat and Water (SHAW) model [*Flerchinger and Saxton*, 1989; *Flerchinger et al*., 1996a, 1996b, 2012; *Flerchinger and Pierson*, 1997], the Utah Energy Balance model with vegetation (UEBveg) [*Mahat and Tarboton*, 2012; *Mahat and Tarboton*, 2013; *Mahat et al*., 2013], the Distributed Hydrology Soil Vegetation Model (DHSVM) [*Wigmosta et al*., 1994; *Wigmosta and Lettenmaier*, 1999], and the dynamic TOPMODEL [*Beven and Freer*, 2001; *Peters et al*., 2003; *Page et al*., 2007].

3.1. Vertical Fluxes of Water and Energy

Full details of the vertical flux parameterizations are provided in *Clark et al*. [2015a], with the primary model options in the initial SUMMA implementation summarized in Table 1. For thermodynamics, we consider multiple options for modeling radiation transfer through the vegetation canopy, surface albedo, and within-canopy and below-canopy turbulence. For hydrology, we consider multiple options for modeling canopy interception, canopy transpiration, and storage and transmission of liquid water through the soil. While the current selection of modeling options is necessarily finite, the structure of SUMMA is sufficiently flexible to enable further extension as discussed as part of the broader vision in the first paper.

3.2. Lateral Fluxes of Water

SUMMA is organized using a flexible hierarchical spatial structure, including a collection of grouped response units (GRUs) within the spatial extent of the model domain and a collection of hydrologic response units (HRUs) within each GRU [see *Clark et al*., 2015b, Figure 2]. The lateral fluxes of water in the soil column can be represented in two main ways: First, the HRUs can be hydrologically connected, in which case the lateral flux from an upslope HRU is the inflow to a downslope HRU (note that we use the kinematic approximation where flow depends on topographic slope [*Clark et al*., 2015a]). Second, the HRUs can be hydrologically disconnected, in which case the lateral flux of water from the HRUs is assumed to flow into the river network. In the hydrologically connected implementation, 1D

Table 1. Physical Processes Included in SUMMA

Process	Subprocess	Model Options	References
Radiation absorbed by vegetation canopy and ground surface • Assume a single homogenous canopy layer	Shortwave radiation transmission through the vegetation canopy	Various applications of Beer's law	[*Dickinson*, 1983; *Sellers*, 1985; *Wigmosta et al.*, 1994; *Nijssen and Lettenmaier*, 1999; *Oleson et al.*, 2010; *Mahat and Tarboton*, 2012]
	Snow albedo	Temporally constant albedo decay rate	[*Verseghy*, 1991]
		Temporally variable albedo decay rate, with semi-empirical portrayal of grain growth and dust loading	[*Yang et al.*, 1997]
Within-canopy and below-canopy turbulence • Use of a single canopy layer, representing fluxes from the surface and vegetation canopy to the canopy air space, and from the canopy air space to the upper boundary [*Choudhury and Monteith*, 1988; *Niu et al.*, 2011; *Mahat et al.*, 2013]	Canopy wind profiles	Exponential attenuation of wind speed through the vegetation canopy	[*Choudhury and Monteith*, 1988; *Niu and Yang*, 2004]
		Logarithmic reductions in wind speed below the vegetation canopy	[*Andreadis et al.*, 2009; *Mahat et al.*, 2013]
	Canopy roughness and displacement height	Various empirical functions of exposed vegetation area and canopy height	[*Choudhury and Monteith*, 1988; *Raupach*, 1994]
	Stability corrections	Various formulations based on the bulk Richardson number	[*Anderson*, 1976; *Louis*, 1979; *Mahrt*, 1987]
Heat transfer within snow and soil • Multiple snow and soil layers	Thermal conductivity of snow	Various empirical formulations of snow density	[*Yen*, 1965; *Mellor*, 1977; *Jordan*, 1991; *Sturm et al.*, 1997]
	Thermal conductivity of soil	Based on the volumetric fraction of the constituents	[*Verseghy*, 1991]
Canopy hydrology • Use of a single canopy layer	Canopy drip	Rapid drainage of excess liquid water from the vegetation canopy	[*Bouten et al.*, 1996]
	Throughfall of snow	Interception capacity formulated as different functions of air temperature	[*Hedstrom and Pomeroy*, 1998; *Andreadis et al.*, 2009]
	Unloading of snow	Unloading formulated as a function of intercepted snow and melt drip	[*Hedstrom and Pomeroy*, 1998; *Andreadis et al.*, 2009]
Snow hydrology • Multiple vertical columns, but assume all transmission of liquid water is in the vertical direction	Precipitation phase	Function of wet bulb temperature	[*Marks et al.*, 2013]
	Snow accumulation	Spatially variable drift factors	[*Luce et al.*, 1998; *Winstral et al.*, 2013]
	Snow melt	Depends on surface energy balance and thermal conductivity	[*Anderson*, 1976]
	Storage and transmission of liquid water in the snowpack	Assume gravity drainage	[*Colbeck*, 1976; *Colbeck and Anderson*, 1982]
Subsurface hydrology • Multiple vertical columns, with options to represent lateral flow of water among soil columns and to include a conceptual subterranean aquifer at the base of the soil profile	Infiltration	Represent limitations in infiltration because of excessive precipitation rate, saturated areas, and partially frozen ground	[*Green and Ampt*, 1911; *Wood et al.*, 1992; *Koren et al.*, 1999]
	Vertical redistribution of liquid water within a soil column	Mixed form of Richards' equation implemented using the Van Genuchten closure relations	[*Van Genuchten*, 1980; *Celia et al.*, 1990]
	Lateral flow among soil columns	Function of total column water storage, with power-law hydraulic conductivity profiles	[*Wigmosta et al.*, 1994; *Beven and Freer*, 2001]
	Base flow from the subterranean aquifer	Conceptual power-law representation	[*Liang et al.*, 1994; *Gulden et al.*, 2007]
	Evapotranspiration	Various model representations of stomatal resistance	[*Jarvis*, 1976; *Ball et al.*, 1987; *Niu et al.*, 2011]

vertical solutions for HRUs within the same GRU are calculated from upslope to downslope (for example from hillslope elements to riparian elements). The lateral flow among HRUs is included as a source/sink term in the conservation equation for soil hydrology, see equation (32) in section 4.1.2. In the hydrologically disconnected implementation, there is no lateral inflow into a soil column and the calculation order for the individual HRUs does not matter. Both the hydrologically connected and the hydrologically disconnected implementations use the power-law decrease in saturated hydraulic conductivity. *Clark et al.* [2015a] provides full details of the different representations of lateral flux of water from the soil profile.

An option for the hydrologically disconnected implementation is the addition of a conceptual subterranean aquifer at the base of the soil profile. As discussed as part of the spatial discretization (section 4.1.3), the aquifer can be can be defined either as (1) a distinct aquifer at the bottom of every soil column [*Wood et al.*, 1992] or (2) at a larger spatial scale, in which the aquifer receives drainage from multiple soil columns [*Hay et al.*, 2006]. In both cases, equation (20) does not include the lateral flux of water across aquifers, and baseflow from the single aquifer (in the first case) or multiple aquifers (the second case) is delivered directly to the stream.

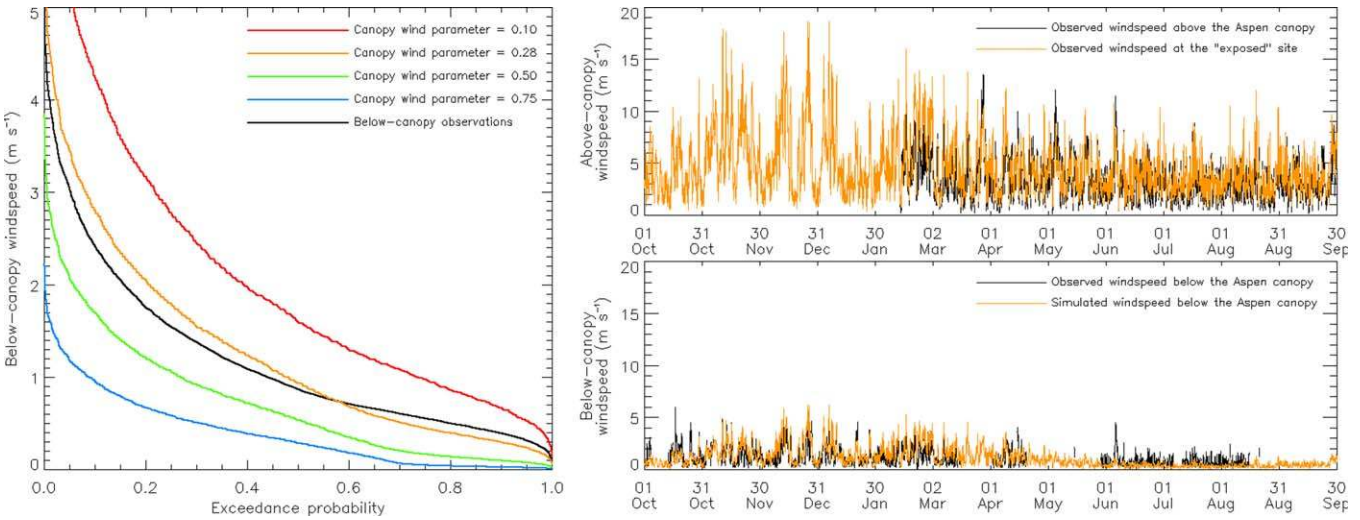

Figure 2. Impact of the choice of the canopy wind parameter, $a_{w,0}$, for the exponential wind profile described in *Clark et al*. [2015a], on simulations of below-canopy wind speed for water year 2006–2007 for the aspen site in the Reynolds Mountain East basin (left plot). The default value of the canopy wind parameter is $a_{w,0} = 0.28$ [*Norman et al*., 1995]. The example time series on the right show the comparison between wind speed measured above the canopy with the serially complete data from the exposed site that is used for model forcing (top), and the comparison between observations and simulations of wind speed below the aspen canopy using the default canopy wind parameter (bottom). The serially complete wind observations at the exposed site are described by *Reba et al*. [2011] and the above-canopy and below-canopy wind observations are described in *Flerchinger et al*. [2012].

4. Model Implementation

Implementing the equations (4), (6), (10), (12), (13), (15), and (20) requires discretization in both space and time. Section 4.1 describes the spatial discretization and section 4.2 describes the temporal discretization (the time stepping scheme).

4.1. Spatial Approximations

4.1.1. Spatial Approximations for the Vegetation Subdomain

The conservation equations for vegetation can be discretized into multiple (vertical) canopy layers. In this paper, we use a single canopy layer (the so-called "big-leaf" model) because it enables comparing approaches used in a wide range of hydrologic and land-surface models [*Liang et al*., 1994; *Lawrence et al*., 2011; *Niu et al*., 2011]. For example, the two-stream canopy shortwave radiation parameterizations [*Dickinson*, 1983; *Mahat and Tarboton*, 2012] and the two-source approach to simulate within-canopy and below-canopy turbulence [*Choudhury and Monteith*, 1988; *Niu et al*., 2011; *Mahat et al*., 2013] are explicitly formulated for a single canopy layer. In the future, these approximations could be relaxed to include multiple canopy layers.

The treatment of the canopy as a single layer (the "big-leaf" model) simplifies the conservation equations as follows. For thermodynamics, equations (4) and (6) simplify to

$$C_p = \frac{\partial T^{veg}}{\partial t} - \rho_{ice} L_{fus} \left[\frac{\partial \theta_{ice}^{veg}}{\partial t} \right]_{mf} = \frac{Q_{swnet}^{veg} + Q_{lwnet}^{veg} + Q_h^{veg} + Q_{sub}^{veg} + Q_{evap}^{veg} + Q_{trans}^{veg}}{D_{can}} \tag{25}$$

$$\rho_{air} c_{air} \frac{\partial T^{cas}}{\partial t} = -\frac{Q_h^{sfc} - Q_h^{total}}{D_{can}} - \frac{Q_h^{veg}}{D_{can}} \tag{26}$$

where $D_{can} = h_{top}^{veg} - h_{bot}^{veg}$ (m) is the depth of the vegetation canopy, Q_{swnet}^{veg} and Q_{lwnet}^{veg} (W m^{-2}) are the shortwave and longwave radiation absorbed by the vegetation canopy, Q_h^{veg} (W m^{-2}) is the sensible heat flux from the vegetation canopy to the canopy air space, and Q_{sub}^{veg}, Q_{evap}^{veg}, and Q_{trans}^{veg} (W m^{-2}) are the latent heat flux associated with canopy sublimation, canopy evaporation and transpiration (Q_h^{veg}, Q_{sub}^{veg}, Q_{evap}^{veg}, and Q_{trans}^{veg} are defined as positive toward the vegetation canopy). Note that the fluxes in equations (25) and (26) are defined per unit area, and relate to the volumetric fluxes in equations (4) and (6) as $Q_h^{veg} = D_{can} H_{sen}^{veg}$, $Q_{sub}^{veg} = D_{can} L_{sub} E_{sub}^{veg}$, $Q_{evap}^{veg} = D_{can} L_{vap} E_{evap}^{veg}$, and $Q_{trans}^{veg} = D_{can} L_{vap} E_{trans}^{veg}$. All other variables are as defined previously.

In contrast to the conservation equations (5), (6), and (7), the formulation in equations (25) and (26) only include state variables for the temperature of the vegetation canopy and the temperature of the canopy air space. This assumes that the canopy air space stores heat (as expressed by the temperature), but not moisture (as expressed by the vapor pressure). This means that the LHS of equation (7) is zero and that the vapor pressure in the canopy air space can be determined as part of the latent heat flux calculations. Treating the vapor pressure in the canopy air space as a diagnostic variable means that equation (7) can be removed from the equation set.

For canopy hydrology, it is convenient to split equation (12) into two separate equations, one for the liquid fluxes and one for the ice fluxes. This greatly simplifies the calculations of melt-freeze needed in the heat equations. The equations can be written for a single canopy layer as

$$\left[\frac{\partial \Theta_m^{veg}}{\partial t}\right]_{liq} = \frac{q_{rf} - q_{tf,rain}^{veg} - q_{drip}^{veg}}{D_{can}} + \frac{Q_{evap}^{veg}}{\rho_{liq} L_{vap} D_{can}} \tag{27}$$

$$\left[\frac{\partial \Theta_m^{veg}}{\partial t}\right]_{ice} = \frac{q_{sf} - q_{tf,snow}^{veg} - q_{unload}^{veg}}{D_{can}} + \frac{Q_{sub}^{veg}}{\rho_{liq} L_{sub} D_{can}} \tag{28}$$

where q_{rf} and q_{sf} (m s^{-1}) define the rainfall and snowfall rates at the top of the canopy, $q_{tf,rain}^{veg}$ and $q_{tf,snow}^{veg}$ (m s^{-1}) define the throughfall of rain and snow through the canopy during precipitation events, q_{drip}^{veg} (m s^{-1}) is the drainage of excess liquid water from the canopy, q_{unload}^{veg} (m s^{-1}) is the unloading of snow through the canopy, and all other variables are as defined previously.

4.1.2. Spatial Approximations for the Snow and Soil Subdomains

The conservation equations in the snow and soil domain describe coupled processes in one vertical dimension (thermodynamics) and three dimensions (hydrology). In this paper, we approximate the snow subdomain as a set of disconnected multilayer vertical columns that drain into the soil subdomain, and we approximate the soil subdomain as a set of hydrologically connected multilayer vertical columns (connected through lateral subsurface flow). The spatial distribution of the snow and soil subdomains and the hydrological connectivity in the soil subdomain offers flexibility to experiment with a broad range of modeling approaches (see section 3.2)—for example, these spatial approximations for the soil subdomain are used in a number of existing catchment hydrology models [e.g., *Wigmosta et al*., 1994; *Beven and Freer*, 2001; *Troch et al*., 2003].

The spatial approximation of the conservation equation for thermodynamics, defined in equation (10), can be written for the j-th layer in the snow-soil subdomain as

$$C_p \frac{\partial T_j}{\partial t} - \rho_{ice} L_{fus} \left[\frac{\partial (\theta_{ice})_j}{\partial t}\right]_{mf} = -\frac{F_{j+1/2} - F_{j-1/2}}{(\Delta z)_j} \tag{29}$$

where $(\Delta z)_j$ (m) is the thickness of the j-th layer. Consistent with the positive downward vertical coordinate, we increment the indices of the snow and soil layers moving downward, meaning that $F^{j+1/2}$ and $F^{j-1/2}$ (W m^{-2}) define the energy flux at the bottom and the top of the layer, respectively. Note that equation (29) is only defined in the vertical dimension (i.e., it is already integrated across the horizontal dimensions), and therefore does not require areal discretization/approximation.

Similar to vegetation, the snow hydrology equations are split into separate equations for liquid and solid fluxes. These can be given for the j-th snow layer as

$$\left[\frac{\partial (\Theta_m^{snow})_j}{\partial t}\right]_{liq} = -\frac{\left(q_{liq,z}^{snow}\right)_{j+1/2} - \left(q_{liq,z}^{snow}\right)_{j-1/2}}{(\Delta z)_j} \tag{30}$$

$$\left[\frac{\partial (\Theta_m^{snow})_j}{\partial t}\right]_{ice} = \begin{cases} \dfrac{q_{tf,snow}^{veg} - q_{unload}^{veg}}{(\Delta z)_j} + \dfrac{Q_{sub}^{sfc}}{\rho_{liq} L_{sub} (\Delta z)_j} & j = 1 \\ 0 & j > 1 \end{cases} \tag{31}$$

where $j = 1$ defines the uppermost snow layer. We include a further simplification that all evaporative losses occur as sublimation and hence we do not include an evaporation term in equation (30).

The fluxes of water between vertical columns in the soil domain is calculated based on the assumption that lateral flow processes can be separated from vertical flow processes (i.e., the Dupuit-Forchheimer assumption). This assumption is reasonable when the rate of subsurface flow is low. Using this assumption, the lateral flux of water is treated as a source/sink term in the state equations for soil hydrology. The spatial approximation of the conservation equations for the storage and transmission of liquid water through soil, as defined in equation (13), can then be written for the vertical dimension as

$$\frac{\partial(\Theta_m^{soil})_j}{\partial t} = -\frac{\left(q_{liq,z}^{soil}\right)_{j+1/2} - \left(q_{liq,z}^{soil}\right)_{j-1/2}}{(\Delta z)_j} + (S_{et})_j - (S_{lf})_j \tag{32}$$

where $(S_{et})_j$ (s^{-1}) is a sink term defining the evapotranspiration losses from the j-th layer and $(S_{lf})_j$ (s^{-1}) is a source/sink term defining the net lateral flux of water in/out of the jth layer. Equation (32) simplifies the 3-D flow processes in equation (13) to enable implementation using a set of soil columns connected by lateral subsurface flow. Note that there is no solid precipitation flux in the soil domain.

4.1.3. The Subterranean Aquifer

As described in section 3.2, a subterranean aquifer can be defined at the bottom of each individual soil column (each HRU) or on a larger spatial scale (multiple soil columns or HRUs drain into a common aquifer). The conceptual subterranean aquifer is only currently implemented for the hydrologically disconnected case (no lateral flow among soil columns or HRUs). This is done because lateral flow is based on the power-law transmissivity profile, where hydraulic conductivity is zero at the base of the soil column [*Clark et al*., 2015a].

4.1.4. Vertical Discretization

SUMMA uses a fixed vertical discretization in the soil and a deforming (time-varying) vertical discretization for snow. The soil is discretized into any number of layers of variable thickness. Typically, thinner soil layers are used near the soil surface to better represent the effects of diurnal temperature forcing [e.g., *Oleson et al*., 2010].

SUMMA's spatial discretization of snow into layers uses a deforming (time varying) vertical grid [*Jordan*, 1991; *Bartelt and Lehning*, 2002; *Oleson et al*., 2010]. The depth of each snow layer is recomputed at the end of each time step, and layers are subdivided or combined when layer depths meet the specific criteria. A snow layer is divided into two when its depth is larger than a prescribed threshold and combined with one of its neighbors when its depth is smaller than a prescribed threshold.

The change in depth of the j-th snow layer over the time interval Δt (s) is given as

$$(\Delta z)_j^{n+1} = \frac{(\theta_{ice})_j^{n+1}}{\left[\Delta t(Q_m)_j/(\rho_{ice}L_{fus}) + (\theta_{ice})_j^{n+1}\right]} \frac{(\Delta z)_j^n}{(1+\kappa_{compact}\Delta t)} + \Delta z_{sfsub} \tag{33}$$

where the superscripts n and $n+1$ define the start and end of the time step, Q_m (W m^{-3}) defines the volumetric rate of snow melt, $\kappa_{compact}$ (s^{-1}) is the rate of snow compaction, and Δz_{sfsub} is the change in the depth of the top layer due to snowfall and sublimation. This change is calculated as

$$\Delta z_{sfsub} = \frac{\rho_{liq}\left(q_{tf,snow}^{veg} + q_{unload}^{veg}\right)\Delta t}{\rho_{s,new}} + \frac{Q_l^{sfc}}{\rho_{liq}L_{sub}(\Delta z)_j} \quad j=1 \tag{34}$$

where $\rho_{s,new}$ (kg m^{-3}) is the density of new snow and Q_l^{sfc} (W m^{-2}) is the latent heat flux at the snow–atmosphere interface. Note that if the vegetation is completely snow covered (or there is no vegetation at all), then $q_{tf,snow}^{veg} = q_{sf}$ and $q_{unload}^{veg} = 0$.

4.2. Temporal Approximation

The spatially discretized conservation equations describe the temporal changes in state variables defined across the spatial model elements. This section describes how to solve these "semi-discrete" equations in time.

The time approximation scheme currently implemented in SUMMA is based on an "operator-splitting" approximation using the implicit Euler scheme. The details of this numerical algorithm are as follows:

1. Operator-splitting approximations are applied to treat the coupled processes separately (sequentially). In particular, each time step is split into two fractional steps: (i) the calculation of solid precipitation fluxes, snow compaction, and sublimation (which affect layer depth), followed by (ii) the calculation of thermodynamic and hydrologic fluxes, including phase change (which affects the temperature and mixture of constituents in each layer). Operator splitting is employed to maintain a fixed vertical grid throughout a single model time step and ensure that the change in ice content over a model time step is only associated with phase change. This greatly simplifies the iterative Newton-Raphson solution of the equations for thermodynamics and liquid water.
2. The fractional steps within the operator splitting approximations are integrated using the implicit Euler scheme, which is applied to equations (35) and (37), as described in section 4.2.2. The implicit Euler approximations are used here because they are unconditionally stable and robust.
3. An adaptive substepping strategy is used to allow for a variable number of "model time steps" (or "substeps") per "forcing data step" [e.g., *Kavetski et al*., 2002; *Clark and Kavetski*, 2010]. Note that forcing data are assumed to be constant throughout a data step, that is, the disaggregation into the model time steps is done uniformly, ignoring substep-scale variability in the forcing.

This time-stepping scheme represents a particular choice of numerical approximation. By separating the numerical solution from the model equations, our overall intent is to provide flexibility in the choice of time stepping scheme. In future work, we envision experimenting with different operator-splitting approximations, different temporal approximations (including higher-order methods), and different adaptive time-stepping strategies. This numerical experimentation will help understand accuracy-efficiency tradeoffs, as well as identify the possible problems associated with the numerical implementation of existing models [*Clark and Kavetski*, 2010; *Kavetski and Clark*, 2010].

4.2.1. Operator-Splitting Approximations

Operator splitting reduces the dimensionality of the solution by splitting the problem into a sequence of operations. The sequence of operations for a given model time step is as follows:

1. Compute terms that are treated as constant over a model time step. These terms include the vegetation phenology (e.g., leaf area index), thermal properties (e.g., volumetric heat capacity and thermal conductivity), surface albedo, and stomatal and soil resistance. Some of these variables may depend on model state variables, but either vary slowly (e.g., volumetric heat capacity and surface albedo) or are costly to compute multiple times over a model time step (e.g., stomatal resistance).
2. Compute terms that do not depend on model state variables. This includes the canopy shortwave radiation fluxes, Q^{veg}_{swnet} and Q^{sfc}_{swnet}, which only depend on the forcing data, vegetation structure, and surface albedo.
3. Compute the change in volumetric ice content on the vegetation canopy from snowfall, throughfall of snow within the vegetation canopy, and unloading of snow from the vegetation canopy.
4. Compute new depth of each snow layer from snow compaction and snowfall, as defined in equations (33) and (34) above, and (if necessary) subdivide and merge snow layers according to the numerical rules defined in section 4.1.4. This action defines the vertical grid used for the solution of the thermodynamic and hydrology calculations in the next step.
5. Solve the temporally discretized equations (35) and (37), as detailed in the next section (section 4.2.2), to compute model state variables T, Θ_m, and ψ_0 at the end of the time step. In solving these equations, we assume that there is no compaction of the snowpack, that the change in ice content associated with sublimation of ice stored on the vegetation canopy and in the snow and soil subdomains is zero, and that the solid precipitation fluxes are zero. This step provides timestep-average water and energy fluxes, such as within-canopy and below-canopy turbulent fluxes (and evapotranspiration), infiltration, and runoff.
6. Compute the change in volumetric ice content in the vegetation and snow domains from the sublimation of ice (based on latent heat fluxes computed in step 5 above).
7. Compute new depth of each snow layer from snow compaction.

Other possible operator-splitting strategies include common approaches in land-surface models in which thermodynamic calculations are split from the hydrology calculations [e.g., *Oleson et al*., 2010], as well as higher order approaches such as Strang splitting [e.g., *Steefel and MacQuarrie*, 1996; *Schoups et al*., 2010].

4.2.2. Implicit Euler Approximations

The implicit Euler approximations for the thermodynamics equations (25), (26), and (29) for domain Ω are

$$C_p\left[\left(T^{\Omega}\right)_j^{n+1}-\left(T^{\Omega}\right)_j^{n}\right]-L_f\rho_{ice}\left[\left(\theta_{ice}^{\Omega}\right)_j^{n+1}-\left(\theta_{ice}^{\Omega}\right)_j^{n}\right]=\frac{\left(F_{net}^{\Omega}\right)_j^{n+1}}{\left(\Delta z\right)_j}\Delta t \tag{35}$$

where n defines the time step index and Δt (s) defines the length of the substep. Note that the second term on the LHS accounts solely for the change in volumetric ice content associated with melt-freeze (see operator splitting approximations listed in section 4.2.1, and ignores changes in ice content associated with sublimation and solid precipitation fluxes (these fluxes are simulated separately).

On the RHS of equation (35), $\left(F_{net}^{\Omega}\right)_j$ (W m^{-2}) is the net flux at the boundaries of the j-th control volume, defined at a given time step (thus dropping the superscript $n+1$) using equations (25), (26), and (29) as

$$\left(F_{net}^{\Omega}\right)_j=\begin{cases} Q_{swnet}^{veg}+Q_{lwnet}^{veg}+Q_h^{veg}+Q_{sub}^{veg}+Q_{evap}^{veg}+Q_{trans}^{veg} & \Omega=veg \\ Q_h^{total}-Q_h^{sfc}-Q_h^{veg} & \Omega=cas \\ F_{j-1/2}-F_{j+1/2} & \Omega=snow,\,soil \end{cases} \tag{36}$$

and $(\Delta z)_j$ is the depth of the j-th control volume, where $(\Delta z)_j = D_{can}$ for the vegetation canopy and the canopy air space. Note the second term on the LHS of equation (35) is zero for the canopy air space because the only constituent is air (i.e., $\theta_{air}^{cas}=1$).

The implicit Euler approximations for the storage and transmission of liquid water described in equations (27), (30), and (32) are defined for domain Ω as

$$\left[\left(\Theta_m^{\Omega}\right)_j^{n+1}-\left(\Theta_m^{\Omega}\right)_j^{n}\right]_{liq}=\frac{\left(q_{net}^{\Omega}\right)_j^{n+1}}{\left(\Delta z\right)_j}\Delta t \tag{37}$$

The net fluxes on the RHS of equation (37) are defined as

$$\left(q_{net}^{\Omega}\right)_j=\begin{cases} q_{rf}-q_{drip}^{veg}+Q_{evap}^{veg}/\left(\rho_{liq}L_{vap}\right) & \Omega=veg \\ \left(q_{liq,z}^{snow}\right)_{j+1/2}-\left(q_{liq,z}^{snow}\right)_{j-1/2} & \Omega=snow \\ \left(q_{liq,z}^{soil}\right)_{j+1/2}-\left(q_{liq,z}^{soil}\right)_{j-1/2}+\left[\left(S_{et}\right)_j-\left(S_{lf}\right)_j\right]\left(\Delta z\right)_j & \Omega=soil \end{cases} \tag{38}$$

The implicit Euler discretization converts the system of ordinary differential equations into a system of nonlinear equations. The nonlinear equations (35) and (37) are solved using Newton-Raphson iteration, where every iteration consists of solving the linear system in equation (39) followed by the update in equation (40):

$$\mathbf{J}^{(m)}\Delta\boldsymbol{\zeta}^{(m+1)}=-\mathbf{r}^{(m)} \tag{39}$$

$$\boldsymbol{\zeta}^{(m+1)}=\boldsymbol{\zeta}^{(m)}+\Delta\boldsymbol{\zeta}^{(m+1)} \tag{40}$$

where the superscript m indexes the iterations (not to be confused with the time step index n), $\boldsymbol{\zeta}$ is the model state vector, $\mathbf{r}$ is the error (residual in the mass balance or energy balance over the time step), and $\mathbf{J}$ is its Jacobian matrix, defined for an individual matrix element as

$$J_{i,j}^{m}=\frac{\partial r_i^m}{\partial \zeta_j^m} \tag{41}$$

All elements of $\mathbf{J}$ are computed analytically, which requires computing the derivatives of all fluxes with respect to the relevant model state variables.

The state vector ζ is assembled by alternating between the thermodynamic and hydrologic states as

$$\zeta = \left[(T^{cas}), (T^{veg}), \left(\Theta_m^{veg}\right), (T)_{j=1}, (\Theta_m)_{j=1}, \ldots, (T)_{j=ns}, (\Theta_m)_{j=ns}, (T)_{j=ns+1}, (\psi_0)_{j=ns+1}, \ldots, (T)_{j=nl}, (\psi_0)_{j=nl} \right] \tag{42}$$

where *ns* defines the number of snow layers and *nl* defines the total number of layers (snow + soil). Note that including thermodynamics and hydrology in the same matrix provides a fully coupled solution, which requires calculating derivatives of the hydrologic fluxes with respect to the thermodynamic state variables (i.e., the derivatives of hydrologic fluxes with respect to temperature throughout the vegetation-snow-soil subdomains) and calculating derivatives of the energy fluxes with respect to the hydrologic state variables (i.e., the derivatives of the energy fluxes with respect to the total water content in the vegetation and snow sub-domains and total water matric potential in the soil subdomain).

The ordering of state variables in equation (42) leads to a pentadiagonal Jacobian matrix for all model configurations that do not include the baseflow sink term for individual soil layers (the model configurations that include the baseflow sink term use the full Jacobian matrix). Equation (39) is solved using the Linear Algebra PACKage (LAPACK) using the band-diagonal and general solvers [*Anderson et al*., 1999].

Comparisons of the coupled solution for hydrology and thermodynamics (as described here) with approaches that alternate between the solutions for hydrology and thermodynamics [*Harlan*, 1973; *Flerchinger and Saxton*, 1989], showed that the fully coupled solution was more computationally efficient.

5. Case Studies

This section presents a set of case studies designed to illustrate how SUMMA can be used to evaluate and select alternative process parameterizations (to improve model fidelity) and to pinpoint specific reasons for model weaknesses (to better characterize model uncertainty and prioritize the areas needing more research and development). The experimental design is summarized in section 5.1 and the model results are presented in section 5.2.

5.1. Model Experiments

5.1.1. Overall Science Questions

The implementation of the method of multiple working hypotheses in SUMMA facilitates progress on the following modeling challenges:

1. *identify preferred process parameterizations*: what modeling approaches should be used to represent the dominant biophysical and hydrologic processes at the spatial scale of the model discretization;
2. *specify spatial architecture*: how should the spatial variability of physical processes be represented across a hierarchy of spatial scales, including the complexity of the spatial linkages (hydrologic connectivity) across the landscape;
3. *characterize model uncertainty*: how can we provide insights into the individual sources of model uncertainty, and develop methods to improve the characterization the uncertainty in model predictions.

These questions represent major challenges in the development and application of hydrologic models [*Reggiani et al*., 1998; *Beven*, 2006; *Renard et al*., 2010; *Wood et al*., 2011].

The general SUMMA concept is also useful to evaluate models of varying complexity and to evaluate different numerical solvers. These questions can be addressed in future work by implementing the more parsimonious flux parameterizations used in bucket-style rainfall-runoff models [e.g., from *Clark et al*., 2008] as well as different methods for the numerical solution (e.g., following the general approach described in *Clark and Kavetski* [2010]).

5.1.2. Methodology

The case studies explore how SUMMA can help identify preferable modeling approaches and pinpoint specific reasons for model weaknesses. To this end, we compare model simulations obtained using SUMMA to observations of a suite of biophysical and hydrologic processes at research sites throughout the western USA. Specifically, we use one-at-a-time sensitivity analysis to evaluate the choice of equations used to parameterize specific processes, the choice of parameter values used in the model equations, and the

spatial configuration of the model. The processes we consider include radiation transfer through the vegetation canopy, within-canopy and below-canopy turbulence, canopy interception, canopy transpiration, snow accumulation and ablation, and runoff generation.

Our process-oriented focus enables us to decompose the overall modeling problem into individual process components and evaluate the representations of individual processes and their interactions. We follow two main approaches when comparing model simulations to data:

1. *Isolated process evaluations*. We compare alternative model representations of individual physical processes through the analysis of internal fluxes and state variables. For example, analysis of below-canopy shortwave radiation fluxes can provide insight into the canopy shortwave parameterizations, and analysis of the storage of water on the vegetation canopy can provide insight into the snow interception parameterizations. These isolated process evaluations are conducted using different, but a priori equally plausible, parameter values. This allows us to explore the interplay between the choice of model parameter values and the choice of parameterization of a given process.
2. *Integrated model predictions*. We evaluate the impact of different modeling decisions on system-scale behavior through the analysis of "system-scale" fluxes, that is, analysis of fluxes that depend on multiple thermodynamic and hydrologic processes (e.g., evapotranspiration, basin-wide runoff). Such an integrated model evaluation considers the interplay (and compensatory effects) among the choice of model parameter values and process parameterizations in different parts of the model.

The analysis illustrated here is a first step toward using SUMMA to investigate the three science questions outlined in section 5.1.1. We expect to gain new understanding of the relative importance of the choice of process parameterizations and model parameter values for different biophysical and hydrologic processes, new understanding of the importance of spatial configurations in determining evapotranspiration and runoff fluxes, and new understanding of the limitations of data in effectively discriminating among competing modeling approaches. The analyses presented here are intended to provide a broad overview of model sensitivities and weaknesses of specific modeling approaches. Subsequent in-depth studies are needed to examine the individual processes and emergent behavior in more detail, using carefully designed experiments to expose key modeling capabilities and limitations, and accounting for uncertainty in both model forcing and evaluation data.

5.1.3. Data

The simulations that follow use data from research sites throughout the western USA. The three sites used in this paper include:

1. The Reynolds Mountain East catchment in southwestern Idaho [*Reba et al*., 2009, 2011, 2012, 2014; *Flerchinger et al*., 2012];
2. The Umpqua experimental forest in southern Oregon [*Storck et al*., 2002]; and
3. The Senator Beck basin in southwest Colorado [*Landry et al*., 2014].

The hydroclimatic character of these sites varies from seasonally snow covered for Reynolds Mountain East and the Senator Beck basin to a transient snow regime in the Umpqua experimental forest. Most simulations presented in this paper are performed at Reynolds Mountain East, as this site includes multiple micrometeorological measurements for different land cover types, as well as runoff measured at the outlet of Reynolds Mountain East.

5.2. Results

5.2.1. Energy Fluxes Through Vegetation

5.2.1.1. Radiation Transmission Within the Vegetation Canopy

An important source of predictive differences among hydrologic and land-surface models is the method used to simulate the transmission and attenuation of shortwave radiation through the vegetation canopy. The main inter-model differences stem from (i) the methods used to simulate radiation transmission through homogenous vegetation [*Dickinson*, 1983; *Sellers*, 1985; *Nijssen and Lettenmaier*, 1999; *Mahat and Tarboton*, 2012]; (ii) the methods used to parameterize the impact of the canopy gap fraction on grid-average shortwave radiation fluxes [*Cescatti*, 1997; *Kucharik et al*., 1999; *Niu and Yang*, 2004; *Essery et al*., 2008]; and (iii) the methods used to represent spatial variability in vegetation type [*Koster and Suarez*, 1992;

Bonan et al., 2002]. In this paper, the parameterizations of canopy shortwave radiation are restricted to radiation transmission through homogenous vegetation, as this approach is used in many existing models. Recent advances in modeling the impact of canopy heterogeneity on grid average fluxes [e.g., *Essery et al*., 2008] are not included at this stage in model development, but can easily be accommodated within the SUMMA methodology and will be considered in future work.

Figure 1 compares the model simulations of downwelling shortwave radiation below the vegetation canopy with below-canopy shortwave radiation observations for the aspen site in Reynolds Mountain East. The results in Figure 1 show that the choice of canopy shortwave parameterization with default parameters can result in differences in estimates of below-canopy shortwave radiation of around 50 W m^{-2} at the Aspen site in Reynolds Mountain East (top row of Figure 1). Results also show that relatively small perturbations in leaf area index produce simulations with as much spread as obtained with the different canopy shortwave radiation parameterizatons (compare the top and bottom rows of Figure 1). The differences in predictions computed using the different parameter values underscore the importance of parameter estimation (e.g., methods to relate geophysical attributes to model parameters [*Samaniego et al*., 2010]) and the need to explicitly represent uncertainty in model parameters in model simulations [e.g., *Kuczera*, 1983; *Beven*, 1993; *Montanari and Koutsoyiannis*, 2012].

5.2.1.2. Turbulent Energy Fluxes

Many existing models simulate within-canopy and below-canopy turbulence using the two-source model described by *Choudhury and Monteith* [1988], in which the key recent examples are CLM [*Oleson et al*., 2010], Noah-MP [*Niu et al*., 2011], and UEBveg [*Mahat et al*., 2013]. An important source of inter-model differences is the parameterization of the canopy wind profile. Figures 2 and 3 illustrate how parameterizations of the within-canopy and below canopy wind profile affect the model simulations of turbulent energy fluxes, snow temperature, and the below-canopy snowpack at the aspen site in Reynolds Mountain East (see *Flerchinger et al*. [2012] for details on measurements). These model simulations are conducted to illustrate the importance of both the choice of process parameterization as well as the choice of model parameters.

The simulations in Figure 2 illustrate that perturbations in the canopy wind parameter used to define the exponential canopy wind profile (parameter $a_{w,0}$ defined in *Clark et al*. [2015a]) cause large variability in the simulations of below-canopy wind speed. Although default values of the canopy wind parameter provide a reasonable match to observations (right plot of Figure 2), perturbations in the canopy wind parameter can modify below-canopy wind speed by a factor of five.

The assumed shape of the below canopy wind profile also has an important impact on below-canopy snow melt. The simulations in Figure 3 illustrate two cases. The first case uses an exponential wind profile that extends to the surface (as in *Choudhury and Monteith* [1988] and *Niu and Yang* [2004]), and the second case uses a wind profile that transitions from exponential to logarithmic at a prescribed height above the ground surface (as in *Andreadis et al*. [2009] and *Mahat et al*. [2013]). The first case results in a higher friction velocity at the surface, which leads to a substantial sensible heat flux directed toward the snow surface, higher temperature of the top snow layer, and, importantly, complete melt of the midwinter snowpack (Figure 3). These modeling decisions that define the shape of the canopy wind profile substantially alter the seasonal cycle of snow melt, and, consequently, water availability during the growing season, transpiration rates, and the overall partitioning of precipitation between evapotranspiration and runoff.

5.2.2. Canopy Interception

Existing models differ substantially in the parameterization of snow interception. In this case study, we use SUMMA to compare the functional behavior of the *Hedstrom and Pomeroy* [1998] and *Andreadis et al*. [2009] parameterizations of snow interception capacity (both parameterizations are described in *Clark et al*. [2015a]).

Figure 4 shows that the *Hedstrom and Pomeroy* [1998] and *Andreadis et al*. [2009] parameterizations exhibit opposite behavior. In particular, *Hedstrom and Pomeroy* [1998] use a function where interception efficiency *decreases* with air temperature, while *Andreadis et al*. [2009] use a function where interception efficiency *increases* with air temperature. Such pronounced differences in model construction and behavior likely occur because the different parameterizations were developed based on data from different environments. *Hedstrom and Pomeroy* [1998] based their parameterization on data from the cold boreal forest in

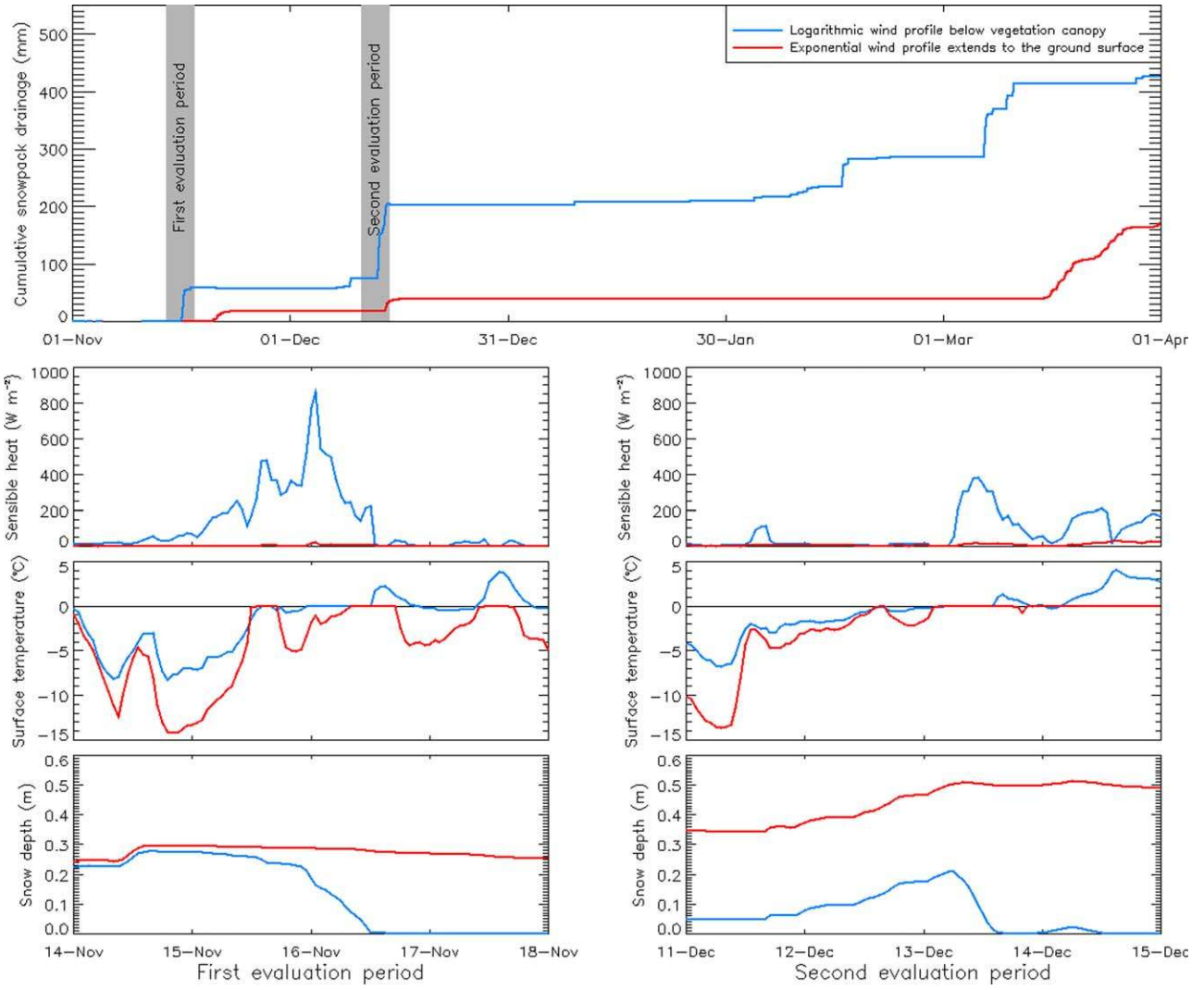

Figure 3. Impact of the choice of below-canopy wind profile on midwinter snow melt during water year 2006–2007 at the aspen site in Reynolds Mountain East basin, showing (top) the cumulative snowpack drainage; and (bottom) the sensible heat flux, surface temperature, and snow depth for two detailed evaluation periods when there is strong snow melt (left and right bottom). The two evaluation periods illustrate that the below-canopy exponential wind profile has much stronger sensible heat flux directed toward the snow surface, leading to warmer surface temperatures and complete melt of the midwinter snowpack.

Saskatchewan, Canada, and *Andreadis et al*. [2009] based their parameterization on data from a warm maritime snow environment in southern Oregon, USA.

Figure 5 illustrates a direct evaluation of model simulations of snow interception by comparing the simulations of intercepted snow against measurements from the weighing tree experiments at Umpqua conducted by *Storck et al*. [2002]. These simulations use the "default" parameter values of branch interception capacity given by *Mahat and Tarboton* [2013] and *Andreadis et al*. [2009], as well as the default parameter values multiplied by a factor of 2 to demonstrate the impacts of parameter values on the interception simulations.

In terms of interparameterization differences, Figure 5 shows that the *Andreadis et al*. [2009] parameterization does intercept more snow than the *Hedstrom and Pomeroy* [1998] parameterization, especially during larger storms. This occurs primarily because the branch interception capacity at the Umpqua site is higher in the *Andreadis et al*. [2009] parameterization, as air temperatures at Umpqua are close to freezing (note also that the *Andreadis et al*. [2009] parameterization was developed using the data from Umpqua). Figure 4 also shows that (in some storms) the increase in intercepted snow associated with doubling the default interception capacity parameters can have a pronounced impact on the amount of snow stored in the canopy, again emphasizing the importance of selecting appropriate model parameter values.

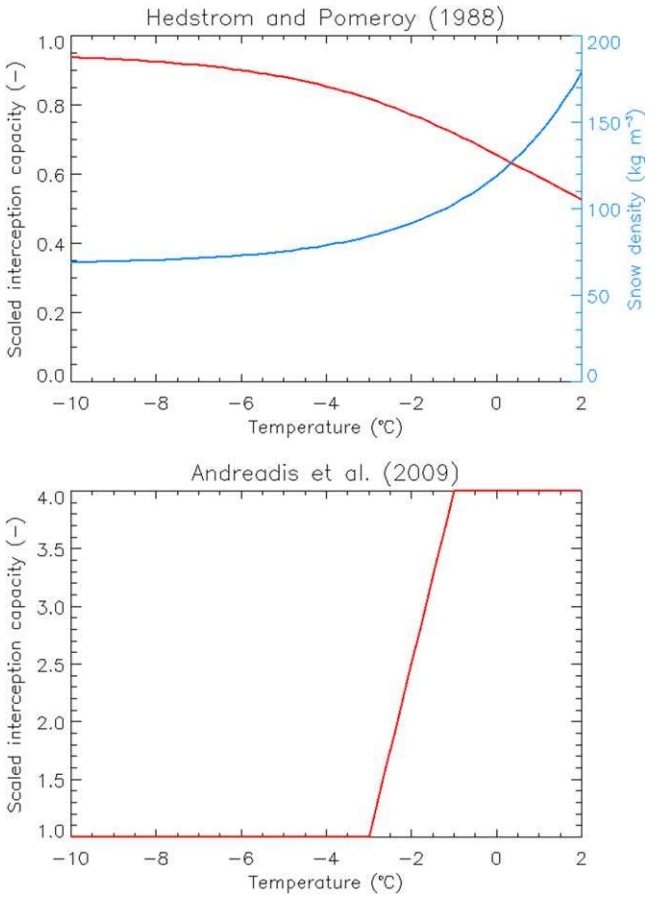

Figure 4. Form of different interception capacity parameterizations (red lines), showing the parameterizations described by (top) *Hedstrom and Pomeroy* [1998], and (bottom) *Andreadis et al.* [2009], as described in *Clark et al.* [2015a]. Note that the *Hedstrom and Pomeroy* [1998] parameterization is a function of new snow density, which, in turn, is a function of air temperature—the relationship between new snow density and air temperature is shown as the blue line in the top plot.

5.2.3. Snow Albedo Effect on Accumulation and Melt in Clearings

Another important source of differences in predictive behavior arises from the methods used to parameterize snow albedo [*Essery et al.*, 2013]. Different model representations of snow albedo include (1) semi-empirical parameterizations to describe the temporal decay in snow albedo after snowfall events [e.g., *Verseghy*, 1991; *Yang et al.*, 1997], and (2) more physically realistic approaches that (i) explicitly simulate the growth of snow grains [e.g., *Wiscombe and Warren*, 1980; *Jordan*, 1991; *Tribbeck et al.*, 2006] and (ii) explicitly simulate the deposition, burial, and re-emergence of atmospheric aerosols (e.g., soot, dust) and forest litter, and the impacts of soot, dust and forest litter on absorption of solar radiation at different depths in the snowpack [e.g., *Warren and Wiscombe*, 1980; *Hardy et al.*, 2000; *Flanner et al.*, 2007]. In this paper, we follow the approaches used in *Niu et al.* [2011] and restrict the attention to two widely used semi-empirical albedo parameterizations – the Biosphere–Atmosphere Transfer Scheme (BATS) described by *Yang et al.* [1997], where the albedo decay rate varies over time, and the Canadian Land Surface Scheme (CLASS) described by *Verseghy* [1991], where the albedo decay rate is fixed in time. The BATS albedo parameterization is used in CLM3.0 and UEBveg, and a parameterization similar to CLASS is used in VIC [*Andreadis et al.*, 2009]. *Clark et al.* [2015a] provide specific details on these albedo formulations.

We examine the impact of the model representation of snow albedo on simulations of snow depth using data from the sheltered sites in the Reynolds Mountain East and Senator Beck basins. Both of these sites are located in a forest clearing, where the grasses are buried by snow early in the snow season and vegetation has a limited impact on the seasonal evolution of snow depth. Moreover, both of these sheltered sites have low wind speeds [*Reba et al.*, 2011; *Landry et al.*, 2014], and turbulent heat fluxes have a small impact on the surface energy balance. The limited importance of canopy snow processes and turbulent heat fluxes at these sheltered sites means that the seasonal evolution of the snowpack is largely controlled by the surface radiation budget. These sheltered sites are therefore ideal to evaluate how parameterizations of snow albedo affect aggregate model behavior.

Figure 6 shows modeled snow depth based on different albedo decay parameterizations. The differences between the model and the observations are larger in the Senator Beck basin than in Reynolds Mountain East. In particular, the model simulations in Senator Beck do not capture the rapid springtime melt that is

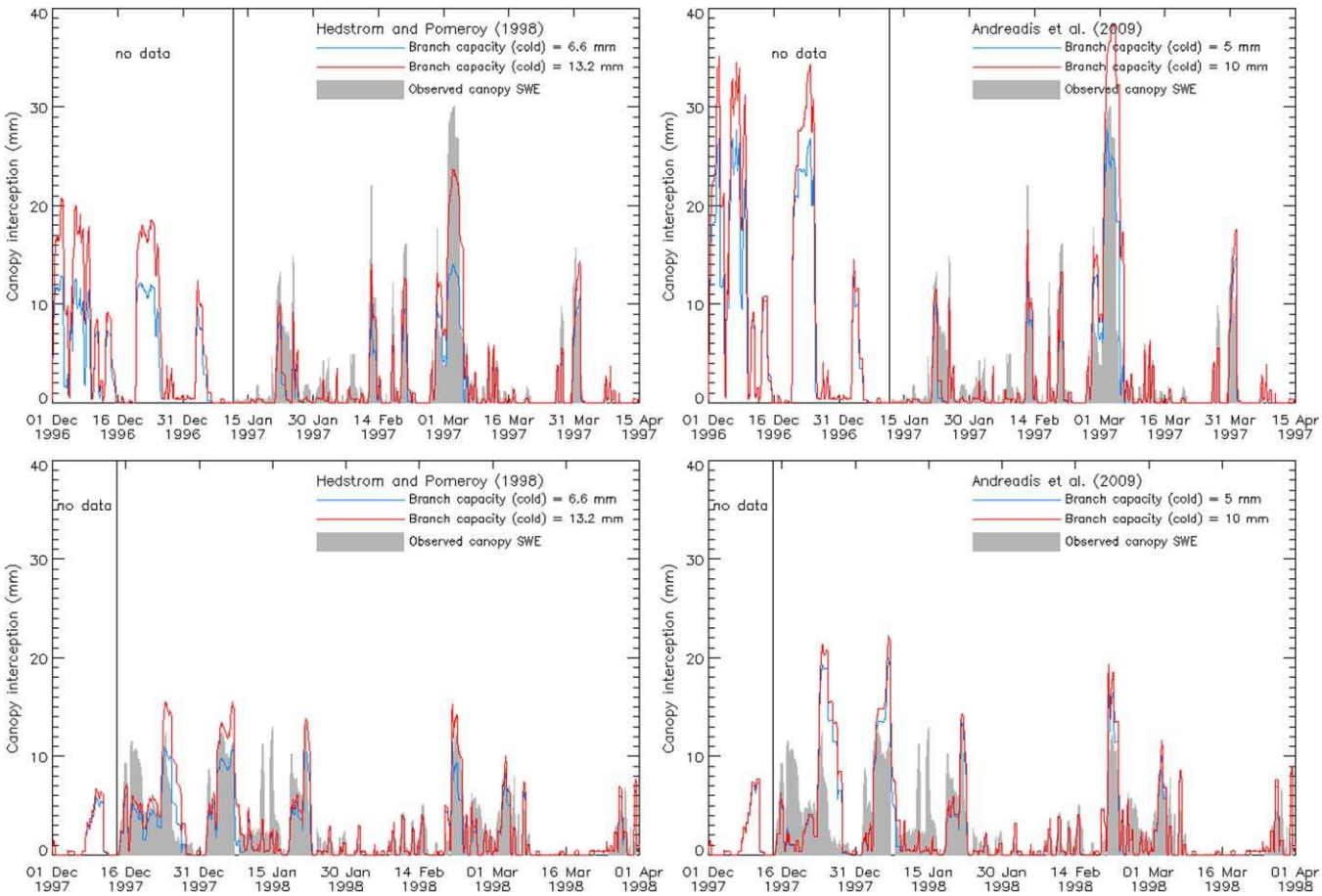

Figure 5. Impacts of model parameters and model parameterizations on simulations of intercepted SWE at the Umpqua site, for water year 1996–1997 (top) and water year 1997–1998 (bottom), using the *Hedstrom and Pomeroy* [1998] parameterization (left) and the *Andreadis et al*. [2009] parameterization (right), for different values of the branch interception parameter (red and blue lines). The branch interception capacity parameter—$\bar{I}_{b,ice}$ (kg m^{-2}) in the *Hedstrom and Pomeroy* [1998] parameterization, and m (kg m^{-2}) in the *Andreadis et al*. [2009] parameterization [see *Clark et al*., 2015a]—defines the interception capacity under cold conditions. The observed canopy SWE (gray shading) is from the weighing tree experiments described by *Storck et al*. [2002].

evident in the observations. These model errors can possibly be attributed to the strong dust loading in the Senator Beck basin [*Painter et al*., 2012], which may not be adequately represented in the snow albedo parameterizations and snow albedo parameters. An interesting result is that the simulations using the BATS (variable decay rate) and CLASS parameterizations (constant decay rate) are almost indistinguishable. The results presented in Figure 6, while clearly case specific, underscore a key issue that is important for model development: The differences among the competing snow albedo parameterizations do not capture the uncertainty in model simulations (e.g., as evident in Figure 6, both the BATS and CLASS parameterizations get the wrong results for the same reasons). This provides an interesting example where ensembles of process parameterizations (with fixed "default" parameter values) may be unsuitable as a proxy for model uncertainty.

5.2.4. Soil Hydrology

5.2.4.1. Evapotranspiration

The total evapotranspiration flux depends on many thermodynamic and hydrologic processes. The modeled fraction of net radiation that contributes to transpiration is governed primarily by stomatal resistance, which, in many environments, is strongly influenced by model representations of soil hydrology. In this paper, we include different model representations of stomatal resistance, including different soil stress functions [*Niu et al*., 2011] and different approaches to simulate biophysical controls on stomatal resistance [*Jarvis*, 1976; *Ball et al*., 1987]. The different soil stress functions and stomatal resistance parameterizations are detailed in *Clark et al*. [2015a].

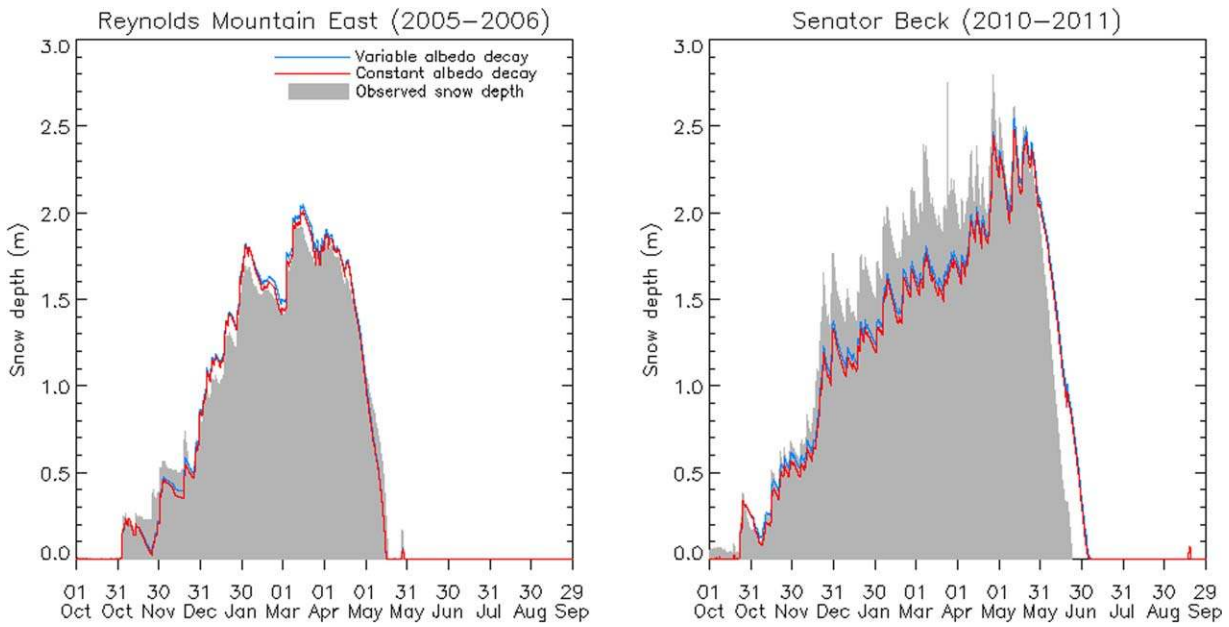

Figure 6. Impact of the choice of model parameterizations on simulations of snow depth for an example water year at the sheltered sites within the Reynolds Mountain East basin (left) and Senator Beck basin (right). The model simulations use the default parameters for the BATS (variable decay rate) and CLASS parameterizations (constant decay rate) in Noah-MP [*Niu et al*., 2011]. The observations of snow depth (shading) are described by *Reba et al*. [2011] for Reynolds Creek, and by *Landry et al*. [2014] for Senator Beck.

For the model experiments, we first evaluate the sensitivity of evapotranspiration to different model representations of stomatal resistance, and then evaluate different model representations of rooting profiles, soil stress functions, and the lateral flux of liquid water among soil columns. Model-data comparisons are shown for the above-canopy aspen eddy-covariance site in Reynolds Mountain East for the time period 1 June 2007 until 20 August 2007.

5.2.4.1.1 Sensitivity to Stomatal Resistance Parameterizations

The simulations in Figure 7 illustrate substantial differences in the estimates of the diurnal cycle of transpiration depending on the choice of stomatal resistance parameterization. The simple soil resistance parameterization [*Liang et al*., 1994], when combined with the two-source model of within-canopy and below-canopy turbulence [*Choudhury and Monteith*, 1988; *Clark et al*., 2015a], results in a substantial amount of transpiration at night when there is no light available for photosynthesis. The physiological representations of transpiration – using the Jarvis and Ball-Berry parameterizations, as defined in *Clark et al*. [2015a] – have an explicit dependence on photosynthetically active radiation and show the expected result of zero transpiration during nighttime hours, resulting in a poor match with observations (Figure 7).

A striking result from Figure 7 is that the Ball-Berry parameterization underestimates evapotranspiration when applied using the default model parameters for stomatal resistance in combination with the particular choice of process parameterizations and parameters for soil hydrology. Note that the soil hydrology options used here are consistent with traditional land-surface models, using a single soil column with uniform hydraulic conductivity, uniform root distribution, no lateral flow, and the Noah-type soil stress function. A key question is how the process parameterizations in one part of the model depend on the choice of process parameterizations and parameters in other parts of the model. The impacts of the choice of stomatal resistance parameters on total evapotranspiration were examined by *Bonan et al*. [2011], and the impacts of the choice of process parameterizations and parameters for soil hydrology on the total evapotranspiration are examined in the next section.

5.2.4.1.2 Sensitivity to Parameterizations of Root Distributions and the Lateral Flux of Liquid Water

Figure 8 illustrates the sensitivity of evapotranspiration to the distribution of roots (left plot), which dictates the capability of plants to access water, and the model representation of the lateral flux of liquid water (right plot), which determines (in part) the availability of soil water. The simulations in Figure 8 have the

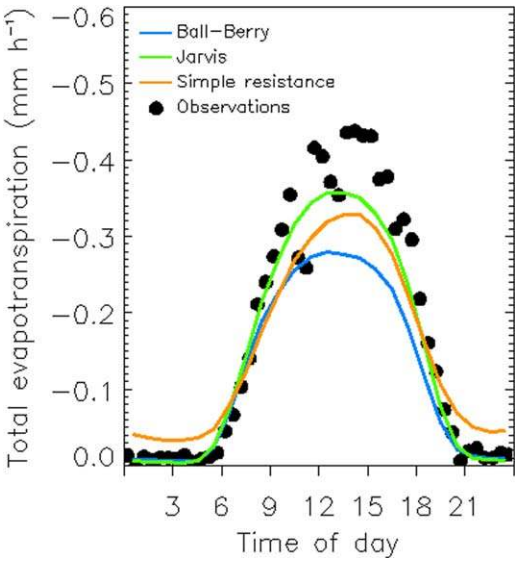

Figure 7. Impact of the choice stomatal resistance parameterizations on simulations of total evapotranspiration at the aspen site in Reynolds Mountain East for the intensive study period in the 2007 growing season (1 June until 20 August) studied by *Flerchinger et al.* [2012]. The observations (circles) are from eddy-correlation measurements from a tower above the Aspen stand.

Ball-Berry parameterization as the reference parameterization for all subsequent perturbations. This is done in part because it is the most complex parameterization and in part to evaluate the impact of compensatory errors in different parts of the model.

The results in Figure 8 demonstrate strong sensitivities both the rooting profile and the lateral flow parameterization. Lower root distribution exponents place more roots near the surface. This makes it more difficult for plants to extract soil water lower in the soil profile, and decreases transpiration (left plot of Figure 8). There is also strong sensitivity to the parameterization of the lateral flux of liquid water. The parameterizations based on power-law transmissivity profiles (both lumped and distributed) have more drainage of soil water at deeper soil layers; however, the distributed simulations include inflow from upslope, resulting in more plant-available soil water and an increase in transpiration. Taken together, the results in Figure 8 illustrate the strong interdependencies among different modeling decisions, which of course complicate discriminating among competing process parameterizations.

5.2.4.2. Basin-Wide Runoff

Basin-wide runoff is a challenging variable to evaluate: it is the integrated response of the system to external forcing and, as such, represents an aggregation of many thermodynamic and hydrologic processes.

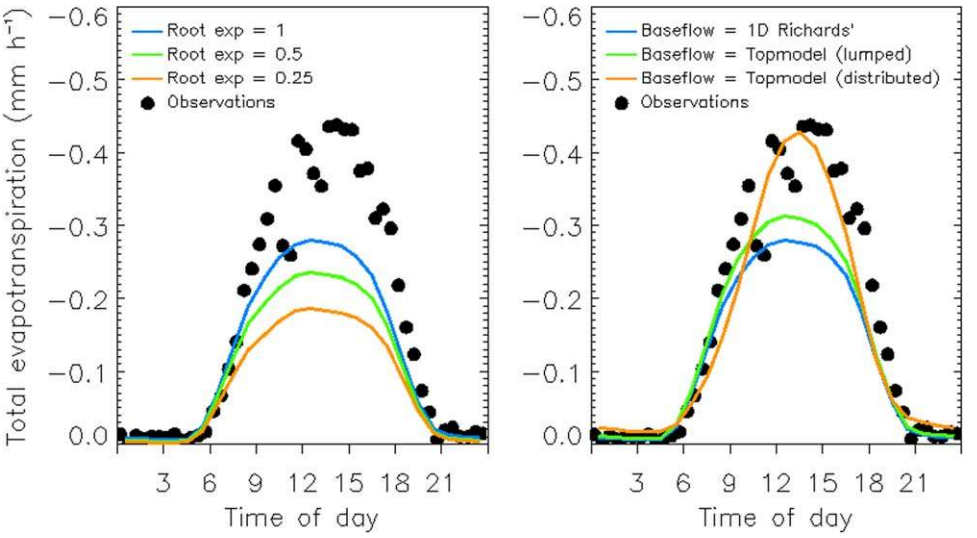

Figure 8. Impact of the parameter values and process parameterizations on simulations of total evapotranspiration at the aspen site in Reynolds Mountain East for the intensive study period in the 2007 growing season (1 June until 20 August) studied by *Flerchinger et al.* [2012], showing (left) the impact of the root distribution and (right) the lateral flux parameterization. The blue line is the same as in Figure 7 (Ball-Berry stomatal conductance, uniform root distribution, and free-draining vertical soil column). The observations (circles) are from the eddy-correlation measurements described in *Flerchinger et al.* [2012].

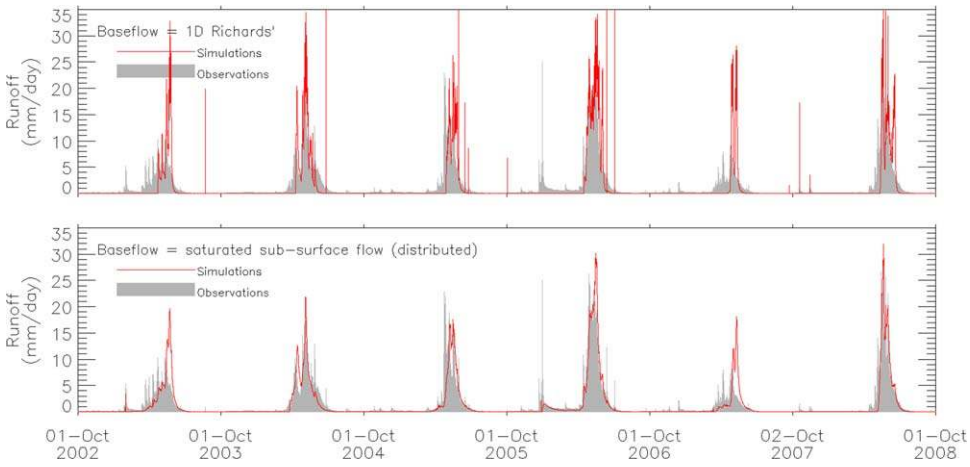

Figure 9. Impact of different lateral flux parameterizations on simulations of runoff (red lines) for the Reynolds Mountain East basin, showing (top) the 1-d Richards parameterization and (bottom) the spatially distributed saturated subsurface flow parameterization. The runoff observations (shading) are described by *Reba et al*. [2011].

Nevertheless, the fingerprint of different parameterizations to simulate lateral fluxes of liquid water are often clearly evident in the basin-wide runoff time series [e.g., *Yilmaz et al*., 2008; *Clark et al*., 2009], and there is much valuable information content in the runoff time series itself [*Clark et al*., 2011]. In addition, streamflow is often the most accurately measured, spatially integrated component of the hydrological cycle. Here, we compare the model simulations of runoff from a small subset of model options to the observations in the Reynolds Mountain East watershed across multiple water years [*Reba et al*., 2011]. The subset of model options is selected to illustrate the different types of model behavior, rather than provide an exhaustive analysis of all modeling alternatives.

Figure 9 illustrates that simulations of basin-wide runoff strongly depend on the model representation of lateral flow. Simulations based on the 1D Richards equation exhibit too many "spikes" in the hydrograph (top plot of Figure 9). In this approach, common in traditional land-surface models [e.g., *Chen and Dudhia*, 2001], there is no explicit representation of lateral flow – i.e., the source/sink term for lateral subsurface flow in equation (32) is set to zero – and vertical drainage from the bottom of the soil profile is delivered immediately to the stream. This exceedingly spiky behavior occurs because the model does not include the longer residence times present in natural systems. The spatially distributed simulations – i.e., including lateral flow among soil columns – represent the observations reasonably well, without the ephemeral behavior in the 1D Richards solution (bottom plot of Figure 9). In these distributed simulations, multiple hillslope soil columns contribute inflow to the riparian zone, resulting in the persistence of partially saturated soils in the riparian zone and smoother (less spiky) runoff dynamics that are consistent with the observations.

6. Conclusions

This two-part paper develops and applies a unified approach to hydrologic modeling, the SUMMA. SUMMA is based on the current community understanding of how the dominant fluxes of water and energy affect the time evolution of thermodynamic and hydrologic states, and provides a general set of conservation equations with the capability to incorporate multiple choices for different flux parameterizations. The first paper [*Clark et al*., 2015b] presents the general modeling concept. This second paper presents the conservation equations and their spatial approximations, describes multiple parameterizations for different biophysical and hydrologic processes, and uses data from the research sites throughout the western USA to evaluate alternative process parameterizations, model parameter values, and spatial structures. The SUMMA framework presented here is designed to enable users to decompose the modeling problem into the individual decisions made as part of model development and evaluate different model development decisions in a systematic and controlled way. Our overall intent is to help modelers select among modeling alternatives (to improve model fidelity) and pinpoint specific reasons for model weaknesses (to better characterize model uncertainty and prioritize areas needing more research and development).

The key points of this paper are as follows:

1. The model development in this paper illustrates how different representations of multiple physical processes can be combined within a general modeling framework. We present the development of the SUMMA structural core, including the specification of the conservation equations, the spatial approximations, and the numerical solution. We also briefly summarize the multiple parameterizations for the different thermodynamic and hydrologic fluxes (i.e., the flux terms in the conservation equations) included in the initial implementation of SUMMA, considering different parameterizations for radiation transfer through the vegetation canopy, within-canopy and below-canopy turbulence, canopy interception, canopy transpiration, snow accumulation and ablation, and runoff generation.
2. The case studies illustrate how systematic comparison of multiple modeling approaches can help identify preferable modeling options. Specific examples of preferable modeling approaches include the use of physiological methods to estimate stomatal resistance (Figure 7), careful specification of the shape of the within- and below-canopy wind profile (Figure 3), explicitly accounting for dust concentrations within the snowpack (Figure 6), and explicitly representing distributed lateral flow processes (Figures 8 and 9).
3. The case studies also illustrate that changes in parameter values can make as much or more difference to the model predictions than changes in the process representation (e.g., Figures 1, 5, and 8). These results emphasize that improvements in model fidelity require a sagacious choice of both process parameterizations and model parameters. While identifying suitable model parameter values and process parameterizations is very difficult given limited and highly uncertain data, SUMMA enables progress on the model identification problem. SUMMA provides scope to both cherry-pick the most preferable physics options from multiple existing models (rather than forcing the modeler to select a single entire model) and the flexibility to adjust model parameter values to represent local site characteristics, all done in a framework that can control for process interactions and compensatory errors.
4. From an uncertainty perspective, the case studies expose the range in predictive behavior that arises from specific choices of process parameterizations and model parameter values (e.g., radiation transmission, differing controls on stomatal conductance). SUMMA can be used to build ensembles of process parameterizations and model parameter sets. However, when implementing this approach care must be taken to ensure model has sufficient process representation so that model parameter ensembles are physically meaningful. Parameter ensembles are clearly less useful if the model is based on inadequate process representations (e.g., a temperature-index snow model that uses the same temperature–melt relationship under all conditions), as the ensemble of parameters cannot represent the different magnitude of uncertainty in different events.
5. There are many cases where it is difficult to select "sufficiently representative" modeling options, and uncertainty characterization is more challenging (i.e., the problem of nonuniqueness, often referred to as "equifinality"). For example, the case studies illustrate the difficulty in identifying one parameterization of snow interception as clearly superior over another, even though the different snow interception parameterizations have very different dependence on air temperature. Ongoing model development efforts on diagnosing and correcting model structural errors, adequately recognizing the role of data uncertainties and compensatory errors in model evaluation, are therefore critical to advance characterization of uncertainty and improve the statistical reliability of model predictions.

The work presented here represents the first application of SUMMA to improve hydrologic models, and there are many additional opportunities to build on this work. First, the model simulations presented here cover a broad range of biophysical and hydrologic processes, and, as such, are necessarily limited in terms of the number of experiments conducted and the number of different environments where the model is applied. Second, the model simulations are based on simple perturbation experiments, and there is considerable scope to implement a more advanced model evaluation strategy in order to more effectively discriminate among competing modeling approaches. Third, the work presented here does not address different modeling options for the numerical solution. Much more research needs to be done to continue exploring the behavior of different biophysical and hydrologic processes and their model representations (including detailed uncertainty analysis). Access to the SUMMA source code and example data sets is provided through the SUMMA website at http://www.ral.ucar.edu/projects/summa.

Acknowledgments
We thank Mary Hill, Michael Barlage, Fei Chen, David Lawrence, and Sean Swenson for comments on an earlier draft of this manuscript, and Cindy Halley-Gotway and Kevin Sampson for their help in producing the figures for the paper. We thank the three anonymous reviewers and Keith Beven for their detailed and constructive comments that substantially improved the manuscript. This work was supported through a contract with the U.S. Army Corps of Engineers, through a Cooperative Agreement with the Bureau of Reclamation, through a grant from the National Oceanic and Atmospheric Administration (NOAA) Modeling Analysis Predictions and Projections (MAPP) program (R4310142), and through a grant from the National Science Foundation (EAR-1215809). The data used in this study are available from the authors upon request.

References

Anderson, E., et al. (1999), *LAPACK Users' Guide*, 3rd ed., Soc. for Ind. and Appl. Math., Philadelphia, Pa.
Anderson, E. A. (1976), A point energy and mass balance model of a snow cover, *NOAA Tech. Rep. NWS 19*, 150 pp., U.S. Natl. Weather Serv., Silver Spring, Maryland, USA.
Andreadis, K. M., P. Storck, and D. P. Lettenmaier (2009), Modeling snow accumulation and ablation processes in forested environments, *Water Resour. Res.*, *45*, W05429, doi:10.1029/2008WR007042.
Ball, J. T., I. E. Woodrow, and J. A. Berry (1987), A model predicting stomatal conductance and its contribution to the control of photosynthesis under different environmental conditions, In: Biggens, J. (Ed.), Progress in photosynthesis research. Martinus Nijhoff Publishers, Dordrecht, the Netherlands, pp. 221–224.
Bartelt, P., and M. Lehning (2002), A physical SNOWPACK model for the Swiss avalanche warning. Part I. Numerical model, *Cold Reg. Sci. Technol.*, *35*(3), 123–145, doi:10.1016/s0165-232x(02)00074-5.
Best, M. J., et al. (2011), The Joint UK Land Environment Simulator (JULES), model description.– Part 1: Energy and water fluxes, *Geosci. Model Dev.*, *4*(3), 677–699, doi:10.5194/gmd-4-677-2011.
Beven, K. (1993), Prophecy, reality and uncertainty in distributed hydrological modeling, *Adv. Water Resour.*, *16*(1), 41–51, doi:10.1016/0309-1708(93)90028-e.
Beven, K. (2006), A manifesto for the equifinality thesis, *J. Hydrol.*, *320*(1–2), 18–36, doi: 10.1016/j.jhydrol.2005.07.007.
Beven, K., and J. Freer (2001), A dynamic TOPMODEL, *Hydrol. Processes*, *15*(10), 1993–2011, doi:10.1002/hyp.252.
Bonan, G. B., S. Levis, L. Kergoat, and K. W. Oleson (2002), Landscapes as patches of plant functional types: An integrating concept for climate and ecosystem models, *Global Biogeochem. Cycles*, *16*(2), doi: 10.1029/2000GB001360.
Bonan, G. B., P. J. Lawrence, K. W. Oleson, S. Levis, M. Jung, M. Reichstein, D. M. Lawrence, and S. C. Swenson (2011), Improving canopy processes in the Community Land Model version 4 (CLM4) using global flux fields empirically inferred from FLUXNET data, *J. Geophys. Res*, *116*, G02014, doi:10.1029/2010JG001593.
Bouten, W., M. G. Schaap, J. Aerts, and A. W. M. Vermetten (1996), Monitoring and modelling canopy water storage amounts in support of atmospheric deposition studies, *J. Hydrol.*, *181*(1–4), 305–321, doi:10.1016/0022-1694(95)02907-9.
Celia, M. A., E. T. Bouloutas, and R. L. Zarba (1990), A general mass-conservative numerical solution for the unsaturated flow equation, *Water Resour. Res.*, *26*(7), 1483–1496, doi:10.1029/90WR00196.
Cescatti, A. (1997), Modelling the radiative transfer in discontinuous canopies of asymmetric crowns. I. Model structure and algorithms, *Ecol. Model.*, *101*(2), 263–274, doi:10.1016/s0304-3800(97)00050-1.
Chen, F., and J. Dudhia (2001), Coupling an advanced land surface-hydrology model with the Penn State-NCAR MM5 modeling system. Part I: Model implementation and sensitivity, *Mon. Weather Rev.*, *129*(4), 569–585, doi:10.1175/1520-0493(2001)129<0569:caalsh>2.0.CO;2.
Choudhury, B. J., and J. L. Monteith (1988), A 4-layer model for the heat budget of homogenous land surfaces, *Q. J. R. Meteorol. Soc.*, *114*(480), 373–398, doi:10.1002/qj.49711448006.
Clark, M. P., and D. Kavetski (2010), Ancient numerical daemons of conceptual hydrological modeling. 1. Fidelity and efficiency of time stepping schemes, *Water Resour. Res.*, *46*, W10510, doi:10.1029/2009WR008894.
Clark, M. P., A. G. Slater, D. E. Rupp, R. A. Woods, J. A. Vrugt, H. V. Gupta, T. Wagener, and L. E. Hay (2008), Framework for Understanding Structural Errors (FUSE): A modular framework to diagnose differences between hydrological models, *Water Resour. Res.*, *44*, W00B02, doi:1029/2007WR006735.
Clark, M. P., D. E. Rupp, R. A. Woods, H. J. Tromp-van Meerveld, N. E. Peters, and J. E. Freer (2009), Consistency between hydrological models and field observations: Linking processes at the hillslope scale to hydrological responses at the watershed scale, *Hydrol. Process.*, *23*(2), 311–319, doi:10.1002/hyp.7154.
Clark, M. P., D. Kavetski, and F. Fenicia (2011), Pursuing the method of multiple working hypotheses for hydrological modeling, *Water Resour. Res.*, *47*, W09301, doi:10.1029/2010WR009827.
Clark, M. P., et al. (2015a), The Structure for Unifying Multiple Modeling Alternatives (SUMMA), version 1: Technical description, NCAR Technical Note NCAR/TN-514+STR, 54 pp., National Center for Atmospheric Research, Boulder, Colo., doi:10.5065/D6WQ01TD.
Clark, M. P., et al. (2015b), A unified approach to process-based hydrologic modeling: 1. Modeling concept, *Water Resour. Res.*, *51*, doi:10.1002/2015WR017198.
Colbeck, S., and E. A. Anderson (1982), The permeability of a melting snow cover, *Water Resour. Res.*, *18*(4), 904–908, doi:10.1029/WR012i003p00523.
Colbeck, S. C. (1976), An analysis of water flow in dry snow, *Water Resour. Res.*, *12*(3), 523–527, doi:10.1029/WR018i004p00904.
Cox, P. M., R. A. Betts, C. B. Bunton, R. L. H. Essery, P. R. Rowntree, and J. Smith (1999), The impact of new land surface physics on the GCM simulation of climate and climate sensitivity, *Clim. Dyn.*, *15*(3), 183–203, doi:10.1007/s003820050276.
Dall'Amico, M., S. Endrizzi, S. Gruber, and R. Rigon (2011), A robust and energy-conserving model of freezing variably-saturated soil, *Cryosphere*, *5*(2), 469–484, doi:10.5194/tc-5-469-2011.
Dickinson, R.E. (1983), Land surface processes and climate-surface albedos and energy balance, *Adv. Geophys.*, *25*, 305–353.
Essery, R., P. Bunting, J. Hardy, T. Link, D. Marks, R. Melloh, J. Pomeroy, A. Rowlands, and N. Rutter (2008), Radiative transfer modeling of a coniferous canopy characterized by airborne remote sensing, *J. Hydrometeorol.*, *9*(2), 228–241, doi:10.1175/2007jhm870.1.
Essery, R., S. Morin, Y. Lejeune, and C. B. Menard (2013), A comparison of 1701 snow models using observations from an alpine site, *Adv. Water Resour.*, *55*, 131–148, doi:10.1016/j.advwatres.2012.07.013.
Fenicia, F., D. Kavetski, and H. H. G. Savenije (2011), Elements of a flexible approach for conceptual hydrological modeling. 1. Motivation and theoretical development, *Water Resour. Res.*, *47*, doi:W11510, 10.1029/2010WR010174.
Flanner, M. G., C. S. Zender, J. T. Randerson, and P. J. Rasch (2007), Present-day climate forcing and response from black carbon in snow, *J. Geophys. Res.*, *112*, D11202, doi:10.1029/2006JD008003.
Flerchinger, G. N., and F. B. Pierson (1997), Modelling plant canopy effects on variability of soil temperature and water: Model calibration and validation, *J. Arid Environ.*, *35*(4), 641–653, doi:10.1006/jare.1995.0167.
Flerchinger, G. N., and K. E. Saxton (1989), Simultaneous heat and water model of a freezing snow-residue-soil system. 1. Theory and development, *Trans. ASAE*, *32*(2), 565–571.
Flerchinger, G. N., J. M. Baker, and E. J. A. Spaans (1996a), A test of the radiative energy balance of the SHAW model for snowcover, *Hydrol. Processes*, *10*(10), 1359–1367, doi:10.1002/(sici)1099-1085(199610)10:10<1359::aid-hyp466>3.0.CO;2-n.
Flerchinger, G. N., C. L. Hanson, and J. R. Wight (1996b), Modeling evapotranspiration and surface energy budgets across a watershed, *Water Resour. Res.*, *32*(8), 2539–2548, doi:10.1029/96WR01240.

Flerchinger, G. N., M. L. Reba, and D. Marks (2012), Measurement of surface energy fluxes from two Rangeland sites and comparison with a multilayer canopy model, *J. Hydrometeorol.*, *13*(3), 1038–1051, doi:10.1175/jhm-d-11-093.1.
Freeze, R. A., and R. Harlan (1969), Blueprint for a physically-based, digitally-simulated hydrologic response model, *J. Hydrol*, *9*(3), 237–258, doi:10.1016/0022-1694(69)90020-1.
Fuchs, M., G. S. Campbell, and R. I. Papendick (1978), Analysis of sensible and latent heat flow in a partially frozen unsaturated soil, *Soil Sci. Soc. Am. J.*, *42*(3), 379–385, doi:10.2136/sssaj1978.03615995004200030001x.
Green, W. H., and G. Ampt (1911), Studies on soil physics. 1. The flow of air and water through soils, *J. Agric. Sci*, *4*(1), 1–24.
Gulden, L. E., E. Rosero, Z. L. Yang, M. Rodell, C. S. Jackson, G. Y. Niu, P. J. F. Yeh, and J. Famiglietti (2007), Improving land-surface model hydrology: Is an explicit aquifer model better than a deeper soil profile? *Geophys. Res. Lett.*, *34*(9), L09402, doi: 10.1029/2007gl029804.
Hardy, J., R. Melloh, P. Robinson, and R. Jordan (2000), Incorporating effects of forest litter in a snow process model, *Hydrol. Processes*, *14*(18), 3227–3237, doi:10.1002/1099-1085(20001230)14:18<3227::aid-hyp198>3.0.CO;2-4.
Harlan, R. (1973), Analysis of coupled heat-fluid transport in partially frozen soil, *Water Resour. Res.*, *9*(5), 1314–1323, doi:10.1029/WR009i005p01314.
Hay, L. E., M. P. Clark, M. Pagowski, G. H. Leavesley, and W. J. Gutowski (2006), One-way coupling of an atmospheric and a hydrologic model in Colorado, *J. Hydrometeorol.*, *7*(4), 569–589, doi:10.1175/jhm512.1.
Hedstrom, N. R., and J. W. Pomeroy (1998), Measurements and modelling of snow interception in the boreal forest, *Hydrol. Processes*, *12*(10–11), 1611–1625, doi:10.1002/(sici)1099-1085(199808/09)12:10/11<1611::aid-hyp684>3.0.CO;2–4.
Jarvis, P. (1976), The interpretation of the variations in leaf water potential and stomatal conductance found in canopies in the field, *Philos. Trans. R. Soc. B*, *273*(927), 593–610, doi:10.1098/rstb.1976.0035.
Jordan, R. (1991), A onedimensional temperature model for a snow cover, *Tech. Doc. for SNTHERM.89*, 49 pp., U.S. Army Corps of Eng. Cold Reg. Res. and Eng. Lab, Hanover, New Hampshire, USA.
Kavetski, D., and M. P. Clark (2010), Ancient numerical daemons of conceptual hydrological modeling. 2. Impact of time stepping schemes on model analysis and prediction, *Water Resour. Res.*, *46*, W10511, doi:10.1029/2009WR008896.
Kavetski, D., P. Binning, and S. W. Sloan (2002), Noniterative time stepping schemes with adaptive truncation error control for the solution of Richards equation, *Water Resour. Res.*, *38*(10), 1211, doi:10.1029/2001WR000720.
Koren, V., J. Schaake, K. Mitchell, Q. Y. Duan, F. Chen, and J. Baker (1999), A parameterization of snowpack and frozen ground intended for NCEP weather and climate models, *J. Geophys. Res*, *104*(D16), 19,569–19,585, doi:10.1029/1999JD900232.
Koster, R. D., and M. J. Suarez (1992), Modeling the land surface boundary in climate models as a composite of independent vegetation stands, *J. Geophys. Res.*, *97*(D3), 2697–2715, doi:10.1029/91JD01696.
Kucharik, C. J., J. M. Norman, and S. T. Gower (1999), Characterization of radiation regimes in nonrandom forest canopies: Theory, measurements, and a simplified modeling approach, *Tree Physiol.*, *19*(11), 695–706, doi:10.1093/treephys/19.11.695.
Kuczera, G. (1983), Improved parameter inference in catchment models. 1. Evaluating parameter uncertainty, *Water Resour. Res.*, *19*(5), 1151–1162, doi:10.1029/WR019i005p01151.
Landry, C. C., K. A. Buck, M. S. Raleigh, and M. P. Clark (2014), Mountain system monitoring at Senator Beck Basin, San Juan Mountains, Colorado: A new integrative data source to develop and evaluate models of snow and hydrologic processes, *Water Resour. Res.*, *50*, 1773–1788, doi:10.1002/2013WR013711.
Lawrence, D. M., et al. (2011), Parameterization improvements and functional and structural advances in Version 4 of the Community Land Model, *J. Adv. Model. Earth Syst.*, *3*, M03001, doi:10.1029/2011MS000045.
Leavesley, G. H., S. L. Markstrom, P. J. Restrepo, and R. J. Viger (2002), A modular approach to addressing model design, scale, and parameter estimation issues in distributed hydrological modelling, *Hydrol. Processes*, *16*(2), 173–187, doi:10.1002/hyp.344.
Liang, X., D. P. Lettenmaier, E. F. Wood, and S. J. Burges (1994), A simple hydrologically based model of land-surface water and energy fluxes for general circulation models, *J. Geophys. Res.*, *99*(D7), 14,415–14,428, doi:10.1029/94JD00483.
Louis, J.-F. (1979), A parametric model of vertical eddy fluxes in the atmosphere, *Boundary Layer Meteorol.*, *17*(2), 187–202, doi:10.1007/bf00117978.
Luce, C. H., D. G. Tarboton, and K. R. Cooley (1998), The influence of the spatial distribution of snow on basin-averaged snowmelt, *Hydrol. Processes*, *12*(10–11), 1671–1683, doi:10.1002/(sici)1099-1085(199808/09)12:10/11<1671::aid-hyp688>3.0.CO;2-n.
Mahat, V., and D. G. Tarboton (2012), Canopy radiation transmission for an energy balance snowmelt model, *Water Resour. Res.*, *48*, W01534, doi:10.1029/2011WR010438.
Mahat, V., and D. G. Tarboton (2013), Representation of canopy snow interception, unloading and melt in a parsimonious snowmelt model, *Hydrol. Processes*, doi:10.1002/hyp.10116.
Mahat, V., D. G. Tarboton, and N. P. Molotch (2013), Testing above- and below-canopy representations of turbulent fluxes in an energy balance snowmelt model, *Water Resour. Res.*, *49*(2), 1107–1122, doi:10.1002/wrcr.20073.
Mahrt, L. (1987), Grid-averaged surface fluxes, *Mon. Weather Rev.*, *115*(8), 1550–1560, doi:10.1175/1520-0493(1987)115<1550:gasf>2.0.CO;2.
Marks, D., A. Winstral, M. Reba, J. Pomeroy, and M. Kumar (2013), An evaluation of methods for determining during-storm precipitation phase and the rain/snow transition elevation at the surface in a mountain basin, *Adv. Water Res.*, *55*, 98–110, doi:10.1016/j.advwatres.2012.11.012.
Maxwell, R. M., and S. J. Kollet (2008), Quantifying the effects of three-dimensional subsurface heterogeneity on Hortonian runoff processes using a coupled numerical, stochastic approach, *Adv. Water Res.*, *31*(5), 807–817, doi:10.1016/j.advwatres.2008.01.020.
Melloh, R. A., J. P. Hardy, R. E. Davis, and P. B. Robinson (2001), Spectral albedo/reflectance of littered forest snow during the melt season, *Hydrol. Processes*, *15*(18), 3409–3422, doi:10.1002/hyp.1043.
Mellor, M. (1977), Engineering properties of snow, *J. Glaciol.*, *19*(81), 15–66.
Montanari, A., and D. Koutsoyiannis (2012), A blueprint for process-based modeling of uncertain hydrological systems, *Water Resour. Res.*, *48*, W09555, doi:10.1029/2011WR011412.
Moore, R., and R. Clarke (1981), A distribution function approach to rainfall runoff modeling, *Water Resour. Res.*, *17*(5), 1367–1382, doi:10.1029/WR017i005p01367.
Nijssen, B., and D. P. Lettenmaier (1999), A simplified approach for predicting shortwave radiation transfer through boreal forest canopies, *J. Geophys. Res.*, *104*(D22), 27,859–27,868, doi:10.1029/1999JD900377.
Niu, G. Y., and Z. L. Yang (2004), Effects of vegetation canopy processes on snow surface energy and mass balances, *J. Geophys. Res.*, *109*, D23111, doi:10.1029/2004JD004884.
Niu, G. Y., and Z. L. Yang (2006), Effects of frozen soil on snowmelt runoff and soil water storage at a continental scale, *J. Hydrometeorol.*, *7*(5), 937–952, doi:10.1175/jhm538.1.

Niu, G. Y., et al. (2011), The community Noah land surface model with multiparameterization options (Noah-MP). 1. Model description and evaluation with local-scale measurements, *J. Geophys. Res.*, *116*, D12109, doi:10.1029/2010JD015139.
Noh, J.-H., S.-R. Lee, and H. Park (2011), Prediction of cryo-SWCC during freezing based on pore-size distribution, *Int. J. Geomech.*, *12*(4), 428–438, doi:10.1061/(asce)gm.1943-5622.0000134.
Norman, J. M., W. P. Kustas, and K. S. Humes (1995), Source approach for estimating soil and vegetation energy fluxes in observations of directional radiometric surface temperature, *Agric. For. Meteorol.*, *77*(3), 263–293, doi:10.1016/0168–1923(95)02265-y.
Oleson, K. W., et al. (2010), Technical description of version 4.0 of the Community Land Model, *NCAR Tech. Note NCAR/TN-478+STR*, p. 257, National Center for Atmospheric Research, Boulder, Colo.
Page, T., K. J. Beven, J. Freer, and C. Neal (2007), Modelling the chloride signal at Plynlimon, Wales, using a modified dynamic TOPMODEL incorporating conservative chemical mixing (with uncertainty), *Hydrol. Processes*, *21*(3), 292–307, doi:10.1022/hyp.6186.
Painter, S. L., and S. Karra (2014), Constitutive model for unfrozen water content in subfreezing unsaturated soils, *Vadose Zone J.*, *13*(4), doi: 10.2136/vzj2013.04.0071.
Painter, T. H., A. P. Barrett, C. C. Landry, J. C. Neff, M. P. Cassidy, C. R. Lawrence, K. E. McBride, and G. L. Farmer (2007), Impact of disturbed desert soils on duration of mountain snow cover, *Geophys. Res. Lett.*, *34*, L12502, doi:10.1029/2007GL030284.
Painter, T. H., S. M. Skiles, J. S. Deems, A. C. Bryant, and C. C. Landry (2012), Dust radiative forcing in snow of the Upper Colorado River Basin. 1. A 6 year record of energy balance, radiation, and dust concentrations, *Water Resour. Res.*, *48*, W07521, doi:10.1029/2012WR011985.
Peters, N. E., J. Freer, and K. Beven (2003), Modelling hydrologic responses in a small forested catchment (Panola Mountain, Georgia, USA): A comparison of the original and a new dynamic TOPMODEL, *Hydrol. Processes*, *17*(2), 345–362, doi:10.1002/hyp.1128.
Pomeroy, J. W., D. M. Gray, T. Brown, N. R. Hedstrom, W. L. Quinton, R. J. Granger, and S. K. Carey (2007), The cold regions hydrological process representation and model: A platform for basing model structure on physical evidence, *Hydrol. Processes*, *21*(19), 2650–2667, doi: 10.1002/hyp.6787.
Raupach, M. (1994), Simplified expressions for vegetation roughness length and zero-plane displacement as functions of canopy height and area index, *Boundary Layer Meteorol.*, *71*(1–2), 211–216, doi:10.1007/bf00709229.
Reba, M. L., T. E. Link, D. Marks, and J. Pomeroy (2009), An assessment of corrections for eddy covariance measured turbulent fluxes over snow in mountain environments, *Water Resour. Res.*, *45*, W00d38, doi:10.1029/2008WR007045.
Reba, M. L., D. Marks, M. Seyfried, A. Winstral, M. Kumar, and G. Flerchinger (2011), A long-term data set for hydrologic modeling in a snow-dominated mountain catchment, *Water Resour. Res.*, *47*, W07702, doi:10.1029/2010WR010030.
Reba, M. L., J. Pomeroy, D. Marks, and T. E. Link (2012), Estimating surface sublimation losses from snowpacks in a mountain catchment using eddy covariance and turbulent transfer calculations, *Hydrol. Processes*, *26*(24), 3699–3711, doi:10.1002/hyp.8372.
Reba, M. L., D. Marks, T. E. Link, J. Pomeroy, and A. Winstral (2014), Sensitivity of model parameterizations for simulated latent heat flux at the snow surface for complex mountain sites, *Hydrol. Processes*, *28*(3), 868–881, doi:10.1002/hyp.9619.
Reggiani, P., M. Sivapalan, and S. M. Hassanizadeh (1998), A unifying framework for watershed thermodynamics: Balance equations for mass, momentum, energy and entropy, and the second law of thermodynamics, *Adv. Water Resour.*, *22*(4), 367–398, doi:10.1016/s0309-1708(98)00012-8.
Renard, B., D. Kavetski, G. Kuczera, M. Thyer, and S. W. Franks (2010), Understanding predictive uncertainty in hydrologic modeling: The challenge of identifying input and structural errors, *Water Resour. Res.*, *46*, W05521, doi:10.1029/2009WRr008328.
Samaniego, L., R. Kumar, and S. Attinger (2010), Multiscale parameter regionalization of a grid-based hydrologic model at the mesoscale, *Water Resour. Res.*, *46*, W05523, doi: 10.1029/2008WR007327.
Schoups, G., J. A. Vrugt, F. Fenicia, and N. C. V. de Giesen (2010), Corruption of accuracy and efficiency of Markov chain Monte Carlo simulation by inaccurate numerical implementation of conceptual hydrologic models, *Water Resour. Res.*, *46*, W10530, doi:10.1029/2009WR008648.
Sellers, P. (1985), Canopy reflectance, photosynthesis and transpiration, *Int. J. Remote Sens.*, *6*(8), 1335–1372, doi:10.1080/01431168508948283.
Simunek, J., N. J. Jarvis, M. T. van Genuchten, and A. Gardenas (2003), Review and comparison of models for describing non-equilibrium and preferential flow and transport in the vadose zone, *J. Hydrol.*, *272*(1–4), 14–35, doi:10.1016/s0022-1694(02)00252-4.
Spaans, E. J. A., and J. M. Baker (1996), The soil freezing characteristic: Its measurement and similarity to the soil moisture characteristic, *Soil Sci. Soci. Am. J.*, *60*(1), 13–19, doi:10.2136/sssaj1996.03615995006000010005x.
Steefel, C. I., and K. T. B. MacQuarrie (1996), Approaches to modeling of Reactive Transport in Porous Media, in *Reactive Transport in Porous Media*, edited by P. C. Lichtner, Mineral. Soc. of Am., Washington, D. C.
Storck, P., D. P. Lettenmaier, and S. M. Bolton (2002), Measurement of snow interception and canopy effects on snow accumulation and melt in a mountainous maritime climate, Oregon, United States, *Water Resour. Res.*, *38*(11), 1223, doi 10.1029/2002WR001281.
Sturm, M., J. Holmgren, M. Konig, and K. Morris (1997), The thermal conductivity of seasonal snow, *J. Glaciol.*, *43*(143), 26–41.
Tribbeck, M., R. Gurney, and E. Morris (2006), The radiative effect of a fir canopy on a snowpack, *J. Hydrometeorol.*, *7*(5), 880–895, doi: 10.1175/jhm528.1.
Troch, P. A., C. Paniconi, and E. van Loon (2003), Hillslope storage Boussinesq model for subsurface flow and variable source areas along complex hillslopes. 1. Formulation and characteristic response, *Water Resour. Res.*, *39*(11), doi:10.1029/2002WR001728.
Van Genuchten, M. T. (1980), A closed-form equation for predicting the hydraulic conductivity of unsaturated soils, *Soil Sci. Soc. Am. J.*, *44*(5), 892–898, doi:10.2136/sssaj1980.03615995004400050002x.
Verseghy, D. L. (1991), CLASS: A Canadian land surface scheme for GCMs. I. Soil model, *Int. J. Climatol.*, *11*(2), 111–133, doi:10.1002/joc.3370110202.
Vidale, P. L., and R. Stockli (2005), Prognostic canopy air space solutions for land surface exchanges, *Theor. Appl. Climatol.*, *80*(2–4), 245–257, doi:10.1007/s00704-004-0103-2.
Warren, S. G., and W. J. Wiscombe (1980), A model for the spectral albedo of snow. II. Snow containing atmospheric aerosols, *J. Atmos. Sci.*, *37*(12), 2734–2745, doi:10.1175/1520-0469(1980)037<2734:amftsa>2.0.CO;2.
Wigmosta, M. S., L. W. Vail, and D. P. Lettenmaier (1994), A distributed hydrology-vegetation model for complex terrain, *Water Resour. Res.*, *30*(6), 1665–1679, doi:10.1029/94WR00436.
Wigmosta, M. S., and D. P. Lettenmaier (1999), A comparison of simplified methods for routing topographically driven subsurface flow, *Water Resour. Res.*, *35*(1), 255–264, doi:10.1029/1998WR900017.
Wiscombe, W. J., and S. G. Warren (1980), A model for the spectral albedo of snow. I: Pure snow, *J. Atmos. Sci*, *37*(12), 2712–2733, doi: 10.1175/1520-0469(1980)037<2712:amftsa>2.0.CO;2.
Winstral, A., D. Marks, and R. Gurney (2013), Simulating wind-affected snow accumulations at catchment to basin scales, *Adv. Water Resour.*, *55*, 64–79, doi:10.1016/j.advwatres.2012.08.011.

Wood, E. F., D. P. Lettenmaier, and V. G. Zartarian (1992), A land surface hydrology parameterization with sub grid variability for general circulation models, *J. Geophys. Res.*, *97*(D3), 2717–2728, doi:10.1029/91jd01786.

Wood, E. F., et al. (2011), Hyperresolution global land surface modeling: Meeting a grand challenge for monitoring Earth's terrestrial water, *Water Res. Res.*, *47*, W05301, doi:10.1029/2010WR010090.

Yang, Z. L., R. E. Dickinson, A. Robock, and K. Y. Vinnikov (1997), Validation of the snow submodel of the biosphere-atmosphere transfer scheme with Russian snow cover and meteorological observational data, *J. Clim.*, *10*(2), 353–373, doi:10.1175/1520-0442(1997)010<0353:votsso>2.0.CO;2.

Yang, Z. L., et al. (2011), The community Noah land surface model with multiparameterization options (Noah-MP). 2. Evaluation over global river basins, *J. Geophys. Res.*, *116*, D12110, doi:10.1029/2010JD015140.

Yen, Y. C. (1965), Effective thermal conductivity and water vapor diffusivity of naturally compacted snow, *J. Geophys. Res.*, *70*(8), 1821–1825, doi:10.1029/JZ070i008p01821.

Yilmaz, K. K., H. V. Gupta, and T. Wagener (2008), A process-based diagnostic approach to model evaluation: Application to the NWS distributed hydrologic model, *Water Resour. Res.*, *44*, W09417, doi:10.1029/2007WR006716.

Zehe, E., H. Lee, and M. Sivapalan (2006), Dynamical process upscaling for deriving catchment scale state variables and constitutive relations for meso-scale process models, *Hydrol. Earth Syst. Sci.*, *10*(6), 981–996.

Zhao, L., D. M. Gray, and D. H. Male (1997), Numerical analysis of simultaneous heat and mass transfer during infiltration into frozen ground, *J. Hydrol.*, *200*(1), 345–363, doi:10.1016/s0022-1694(97)00028-0.